EXPERIMENTAL CHARACTERIZATION OF THE PROPAGATION OF ACOUSTIC WAVES IN PIPE STRINGS

A Thesis

by

AHMED REDISSI

Submitted to the Office of Graduate and Professional Studies of
Texas A&M University
in partial fulfillment of the requirements for the degree of

MASTER OF SCIENCE

Chair of Committee,	Scott Miller
Committee Members,	Erchin Serpedin
	Gregory Huff
	Ding Zhu
Head of Department,	Miroslav Begovic

August 2015

Major Subject: Electrical Engineering

ABSTRACT

This thesis explores the propagation of acoustic waves in pipe strings by designing a series of experimental procedures to characterize their behavior. It describes in detail four sets of experiments that were used to characterize the behavior of the acoustic waves as they propagate in pipe strings. First, the Existence Test tried to prove the existence of the dispersion phenomenon in pipe strings by measuring the speed of waves with different frequencies on a small scale version of the field test bed. Second, the Consistency Test tried to determine the circumstances that allow for reliable and consistent measurements as a preparation for the field tests by testing the transmitter, receiver, and coupling consistency. Third, the Dispersion Test aimed at discovering all of the existing vibrational modes and matching them with the theoretical solutions by performing a two-dimensional Fourier Transform. Finally, the Frequency Test attempted to describe the pipe strings response to both narrowband and broadband signals by proving the existence of passbands and stopbands.

TABLE OF CONTENTS

Page

LIST OF FIGURES

Page

LIST OF TABLES

Page

CHAPTER I

INTRODUCTION AND LITERATURE REVIEW

The propagation of guided acoustic waves in pipe networks has many applications in industry and specifically in the oil and gas industry. Acoustic and ultrasonic waves have been used to perform several inspections to pipe strings since they can detect irregularities such as leaks, damage, and corrosion over long distances. Moreover, the acoustic wave can be used as a replacement for wired communication systems. It offers several advantages over the classic means of communication such as being a low cost substitute to the otherwise high maintenance equipment. It also allows access to pipe strings located in inaccessible areas for both inspection and establishment of communication.

One of the most important tools in the inspection of pipes and in using them as a medium for acoustic waves in order to transmit information is the dispersion relation. Commonly known in physics, the dispersion relation characterizes the relationship between the frequency and the wavenumber or wavelength of a certain wave traversing a medium. Simply put, the dispersion relation makes waves with different frequencies travel at different speeds. In the case of guided waves, the dispersion relation is dictated by three factors: the frequency of the transmitted signal, the geometry of the waveguide, and the material of the waveguide. Knowing these three parameters, one can predict how the wave will behave as it propagates. The dispersion phenomenon will split the wave in

groups of modes where each one is vibrating according to a different wavenumber or wavelength. For a cylindrical waveguide, that is a pipe, there are three possible families of modes: the longitudinal, the flexural, and the torsional modes which will be explained in depth in the next chapter.

A significant number of works has been done in the field of ultrasonic waves. They are commonly used in what is known as Ultrasonic Testing where ultrasonic waves are made to propagate in numerous objects in order to detect anomalies or determine certain material properties [1]. Its main advantage is that it is a non-destructive test that does not cause any harm or damage to the subject that is being tested. Ultrasonic waves have been used to conduct tests and experiment in several industries. They can be used in the aerospace industry [2], in the food industry [3], in the nuclear industry [4], in the oil and gas industry [5], and countless other industries. A good number of ultrasonic testing techniques rely on the use of Lamb waves that can propagate long distance in solid plates. Several techniques have been discovered to optimize these testing procedures [6] and come up with specific excitation techniques [7].

As for acoustic waves, the works of Drumheller have laid the foundations for acoustic waves' propagation in pipe strings and drill strings that are of extreme importance to the drilling and oil and gas industries [8]. Drumheller studied several aspects of this field such as explicitly describing the response of drill strings to acoustic transmission [9] in addition to evaluating their impedance [10]. He also characterized the propagation of

acoustic waves in drill strings [11] and described their attenuation [12], and even studied the case of the presence of fluids in pipe strings [13].

There exists a good number of noteworthy works in the scientific literature that experimented with transmitting acoustic waves in pipe strings [14, 15] and attempted to characterize the channel and its response to different excitation frequencies [16]. Other works studied the phenomenon of the existence of pass-bands and stop-bands in pipe strings [17, 18]. There has also been some more work that explored how acoustic waves propagate in pipe strings filled with liquids such as [19, 20]. Some papers focused on the effect of different types of pipes on the propagation of acoustic waves [21] while others focused on the effect of excitation sources and receiving instruments and built some simulation tools for the study of sound waves [22].

The goal of this work is to design a series of experiments that can characterize the behavior of guided acoustic waves propagating in pipe strings and match it with the theoretical results.

CHAPTER II

GUIDED WAVE PROPAGATION IN PIPES

A guided wave is a wave whose propagation properties such as amplitude, direction, frequency, and wavenumber are dictated by a physical structure called the waveguide. The waveguide not only supports the propagation of different types of waves such as mechanical, acoustic, ultrasonic, and electromagnetic waves but also introduces two major phenomena that distort the traveling wave created by a certain excitation to the waveguide. These two phenomena are the creation of a finite number of propagating modes or patterns of vibration and the dispersion relation between the temporal and spatial characteristics of the wave. As a result, the initial excitation signal will be split into several modes that will travel with different phase and group velocities when observed.

A pipe segment or a network of pipes can be represented as a cylindrical waveguide that will excite certain modes that will in turn travel down the pipe with different frequencies and different wavenumbers causing the existence of dispersion. The types of propagating modes for a cylindrical waveguide and their dispersion relations will be discussed in depth in the next sections.

1. Propagating Modes

Since the pipe can be analytically represented by a hollow cylinder with an inner radius and an outer radius, it seems more suitable to use cylindrical coordinates in order to mathematically describe the system as shown in Figure 2.1.

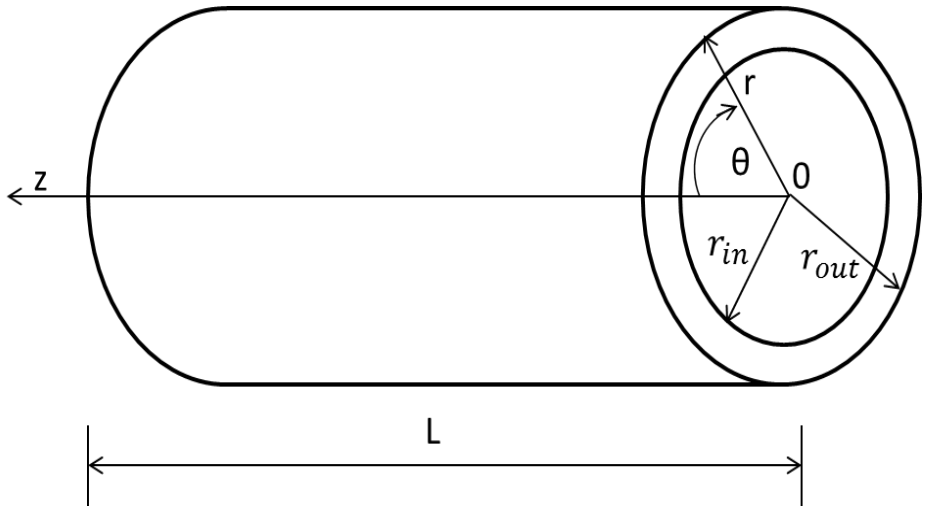

Figure 2.1: Cylindrical coordinate system for a pipe

Any propagating wave will have to adjust to the medium and travel along the three r, z, and θ axes. These modes can be grouped into three families known as the longitudinal, flexural, and torsional modes. Each one of these families of modes is defined by the direction of displacement. The displacement indicates how much, in terms of distance, the wave has traveled from its original position for a given time.

The longitudinal modes have displacements in the r and z direction but none along the θ axis. The torsional modes have displacements in the θ direction and are fixed along the r and z axes. Finally, the flexural modes have displacements in all three directions. Figure 2.2 should help to visualize how each family of modes propagates inside the pipe [23].

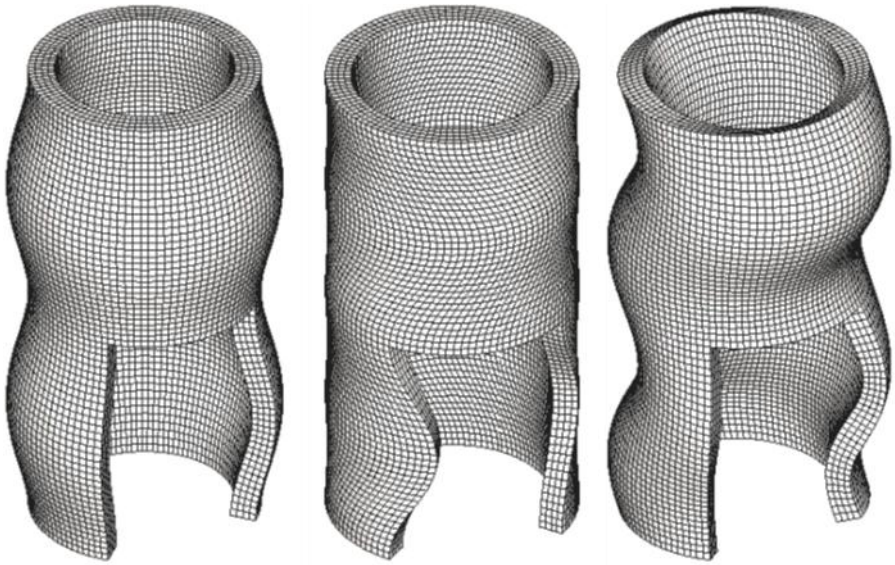

Figure 2.2: Simulation of the three families of modes in a pipe: longitudinal (left), torsional (center), and flexural (right) [23]

2. Dispersion Relation

Dispersion is the effect of the medium on the properties and characteristics of the travelling wave. It is essentially a relation between the frequency and the wavenumber or

wavelength. Consequently, the phase velocity and the group velocity of the wave can be determined for any given frequency. The phase velocity is the rate at which the phase of the wave changes [24]. In other words, it measures how fast the phase changes for a given frequency over a certain propagating distance. On the other hand, the group velocity is the velocity of the envelope or the overall shape of the wave [24, 25]. It measures how much the overall shape of the wave has moved during a certain period of time.

In order to characterize the dispersion relation, the wave equation in cylindrical coordinates must be solved, then the boundary conditions must be applied, and finally the pairs of frequencies and wavenumbers that satisfy the boundary conditions can be found.

Wave propagation in an unbounded isotropic medium can be expressed by the equation of motion as found in [26].

$$\rho \frac{\partial^2 u}{\partial t^2} = \nabla \sigma \tag{2.1}$$

In this equation, u is the three dimensional displacement vector, ρ is the material density of the pipe, σ is the stress tensor, and ∇ is the three dimensional differential operator. The stress tensor can then be related to the strains and displacements by Hooke's Law as:

$$\sigma = \lambda I \nabla u + \mu(\nabla u + (u\nabla)^T) \tag{2.2}$$

In this equation, λ and μ are known as Lame constants [7] and I is the identity matrix. Combining equations (2.1) and (2.2) produces what is known as the Navier equation [26, 27]:

$$\rho \frac{\partial^2 u}{\partial t^2} = (\lambda + \mu)\nabla(\nabla u) + \mu \nabla^2 u \tag{2.3}$$

Using the Helmholtz decomposition, the displacement vector can be decomposed into a scalar potential and a vector potential [26, 27]:

$$u = \nabla \phi + \nabla \times H \text{ with } \nabla . H = 0 \tag{2.4}$$

In this equation, ϕ is the scalar potential and H is the vector potential. Using these potentials and the method of separation of variables, equation (2.3) can be solved and the solution is given by Gazis in [28]. The results for the displacement vector and the stress tensor are [29]:

$$u(r, \theta, z) = u(r) e^{jn\theta} e^{jkz} \tag{2.5}$$

$$\sigma(r, \theta, z) = \sigma(r) e^{jn\theta} e^{jkz} \tag{2.6}$$

In equations (2.5) and (2.6), k represents the wavenumber and n is called the circumferential order which determines the symmetry of the solutions in the azimuthal or θ direction.

The radial parts of both the displacement vector and the stress tensor can be further expressed as follows [29]:

$$u(r) = \begin{bmatrix} u_r(r) \\ u_\theta(r) \\ u_z(r) \end{bmatrix} = D_u \cdot A, \tag{2.7}$$

$$\sigma(r) = \begin{bmatrix} \sigma_{rr}(r) \\ \sigma_{\theta\theta}(r) \\ \sigma_{zz}(r) \\ \sigma_{\theta z}(r) \\ \sigma_{rz}(r) \\ \sigma_{r\theta}(r) \end{bmatrix} = D_\sigma \cdot A, \tag{2.8}$$

$$A = \begin{bmatrix} L_+ \\ L_- \\ SV_+ \\ SV_- \\ SH_+ \\ SH_- \end{bmatrix}. \tag{2.9}$$

The matrix A represents the amplitudes for each direction. L stands for longitudinal, SV stands for shear vertical, and SH stands for shear horizontal. The + and – sign indicate the direction of motion of the wave. The matrices D_u and D_σ are respectively the displacement and stress matrices. Their entries are found in [29, 30] and stated in Appendix A.

The dispersion relation is thus determined by finding the frequency-wavenumber pairs that satisfy the boundary conditions of the waveguide. For a cylindrical waveguide, the

boundary conditions state that there is no stress at the traction part at the inner and outer radii of the pipe. That is, when $r = r_{in}$ and $r = r_{out}$:

$$\begin{bmatrix} \sigma_{rr}(r) \\ \sigma_{r\theta}(r) \\ \sigma_{rz}(r) \end{bmatrix} = \begin{bmatrix} 0 \\ 0 \\ 0 \end{bmatrix} \tag{2.10}$$

This condition will be satisfied when the determinant of the stress matrix is equal to zero at the inner and outer radii. This is known as the Pochhammer-Chree frequency equation as given in [29, 30, 31]. In other words:

$$\det(D_\sigma) = \det\left(\begin{bmatrix} D_{i,j}(r_{in}) \\ D_{i,j}(r_{out}) \end{bmatrix}\right) = 0 \text{ for } i,j = 1,5,6 \tag{2.11}$$

The stress matrix will be different for each family of modes. For the torsional modes, it is simplified to a 2-by-2 matrix since the displacements are in the azimuthal direction only. For the longitudinal modes, it becomes a 4-by-4 matrix since the displacements take place in both the longitudinal and radial directions. As for the flexural modes, the stress matrix is the full 6-by-6 matrix since the displacements are occurring in all directions.

Once the determinant of the stress matrix is calculated, a computer algorithm can search for the frequency-wavenumber pairs that make it go to zero following the change of sign method. For a given frequency, all the wavenumbers that satisfy the boundary conditions and force the determinant of the stress matrix to be equal to zero correspond to the

different modes that are present. A program known as PCDISP in [31] was used to determine the theoretical dispersion curves for the pipe strings used later in the experiments.

CHAPTER III

THE EXISTENCE TEST

1. Experimental Setup for the Existence Test

This test aims at verifying that the pipe can act as a dispersive medium for an acoustic wave. It serves as a small scale version of the Dispersion Test to confirm the assumptions regarding both the existence and the nature of the dispersion phenomenon. Later this test was repeated on the field using pipe segments that were nominally 32 foot long. This test consisted of a series of experiments where a 5 foot long metallic rod was excited using piezoelectric discs that convert electric signals to an acoustic wave. The received signals were recorded using another piezoelectric disc connected to a laptop. Figure 3.1 shows a picture of the piezoelectric discs used for exciting and sensing the acoustic wave and Figure 3.2 shows the experimental setup.

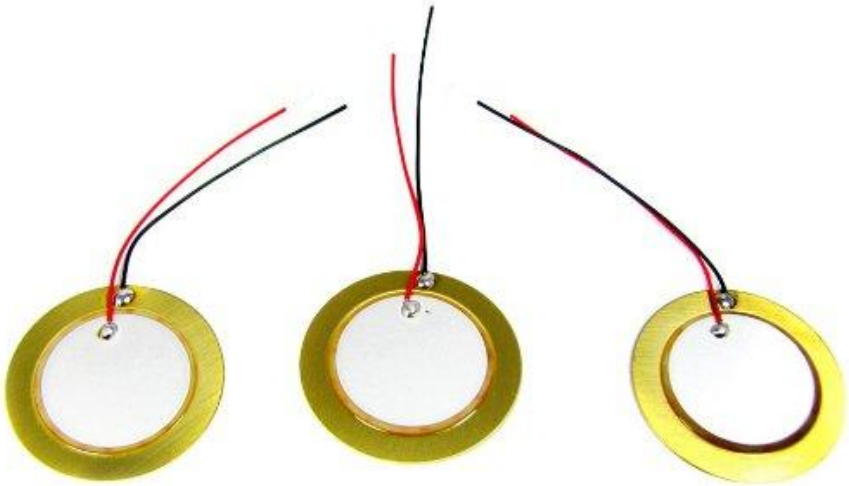

Figure 3.1: Piezoelectric discs used for the Existence Test

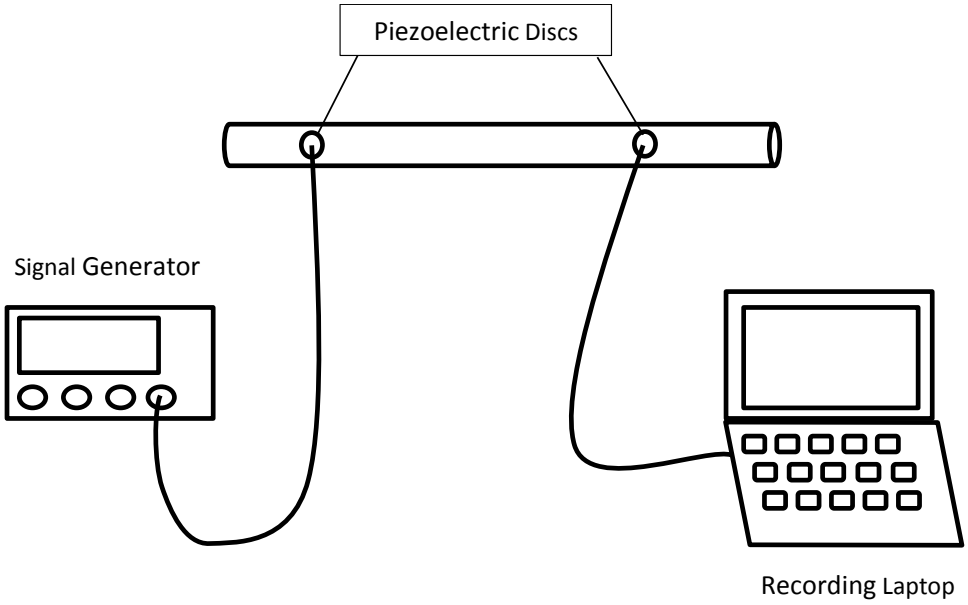

Figure 3.2: Experimental setup for the Existence Test

Once the received signals are recorded, the propagation delay dt between the transmitter and the receiver was measured for a given frequency. The propagation delay can be determined by observing the time when both transmitted and received signals begin to rise above the noise level and subtracting the difference. Figure 3.3 shows how this process is done. The upper plot represents the signal measured in the first position and the lower plot represents the signal measured in the second position. The two positions are separated by a distance dx. The bottom plot has higher amplitude because an accelerometer was used to measure the signal at that position while the piezoelectric disc was used to measure the signal at the first position.

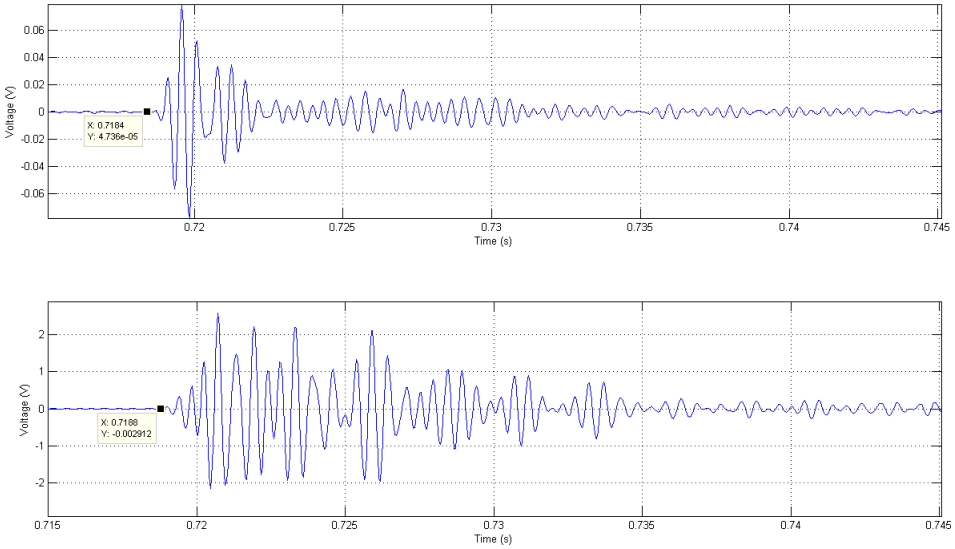

Figure 3.3: Calculation of propagation delay for the Existence Test

$$V_{group} = V_{phase} = \frac{dx}{dt} = \frac{\omega}{k} \tag{3.1}$$

$$k = \frac{\omega}{V_{phase}} = \frac{2\pi f}{V_{phase}} = \frac{2\pi f \cdot dt}{dx} \tag{3.2}$$

$$V_{phase} = \frac{\omega}{k} \tag{3.3}$$

$$V_{group} = \frac{\partial \omega}{\partial k} \tag{3.4}$$

Knowing the propagation distance dx and the propagation delay dt, the group velocity can be calculated. This method can only determine the dispersion for the fastest vibrational mode that is expected to be the longitudinal L(0,1) from the theoretical dispersion curves. The L(0,1) mode behaves linearly at low frequencies, thus the phase and group velocities become equal. The phase velocity can then be determined from equation (3.1) and consequently the wavenumber k can be found from equation (3.2). Therefore, this experiment can determine the dispersion relation for the metallic rod [32]. However, one of the limitations of this experiment is that it can only determine the mode with the fastest travelling frequencies since it only looks at the beginning of the signals.

In order to produce an experimental dispersion curve that is expected to be linear, five data points were produced for 2000, 4000, 6000, 8000, and 10000 Hz. This method suffers from an accuracy issue and is vulnerable to large errors when the propagation delay needs to be estimated. However, it still helps to show that there is a dispersion phenomenon. The next experiments will use a two-dimensional Fourier Transform to produce more accurate dispersion curves.

2. Results of the Existence Test

For low frequencies between 0 and 10 kHz, it is expected that only three modes are present and propagate along a pipe segment. These modes are the first longitudinal L(0,1) mode, the first flexural F(1,1) mode, and the first torsional T(0,1) mode. In the frequency-wavenumber space, it is expected that the T(0,1) behaves linearly for all values, the F(1,1) does not behave linearly for low frequencies, while the L(0,1) behaves linearly for low frequencies. When the dispersion relation is linear or when the curve behaves linearly, the phase velocity and the group velocity defined by equations (3.3) and (3.4) respectively become equal.

As a result, the time difference between the beginnings of the transmitted and received signals which corresponds to the group delay becomes equal to the phase delay. Therefore, for a linear dispersion, it is possible to determine the phase velocity by measuring the group velocity which leads to determining the wavenumber corresponding to a fixed transmit frequency as shown in the previous chapter.

When the pipe was excited using piezoelectric discs and the delay between the transmitted and the received copy of the signal was measured, the frequency-wavenumber pair was found for several data points. The fact that each frequency generated a different wavenumber that increased as the frequency increased meant that there was indeed a dispersion phenomenon occurring in the pipe. The gathered data

points allowed the creation of an experimental dispersion curve that was compared with theoretical curves for all the modes in order to identify which mode was captured.

Figure 3.4 shows the comparison between the theoretical and the experimental curves. The plot shows that the captured mode was the longitudinal L(0,1) since the experimental data points tracked the curve for that particular mode. This is expected as identifying the time of the beginning of the signal meant finding the time delay for the fastest mode which is also the L(0,1) since at a given frequency it vibrates with the smallest wavenumber. The plot not only verified the existence of the dispersion phenomenon but also verified that the metallic rod was made of steel since the theoretical curves were produced for a steel pipe.

For this test, a pipe segment was excited using a broadband pulse. The pulse was filtered using band-pass Bessel filters to isolate different frequencies from the broad spectrum of the signal. The Bessel filter is characterized by a linear phase response which delayed the signals by the same amount, and therefore maintaining the propagation delay constant for each frequency. The filter delay was accounted for during the calculation of each data point and was subtracted from the propagation delay. The filter delay was determined using the group delay plots for each Bessel band-pass filter. Table 3.1 shows the cutoff frequencies for the Bessel band-pass filter for each data point.

Table 3.1: Bessel filters passbands

Center Frequency	Passband
2000 Hz	1500-2500 Hz
4000 Hz	3500-4500 Hz
6000 Hz	5500-6500 Hz
8000 Hz	7500-8500 Hz
10000 Hz	9500-10500 Hz

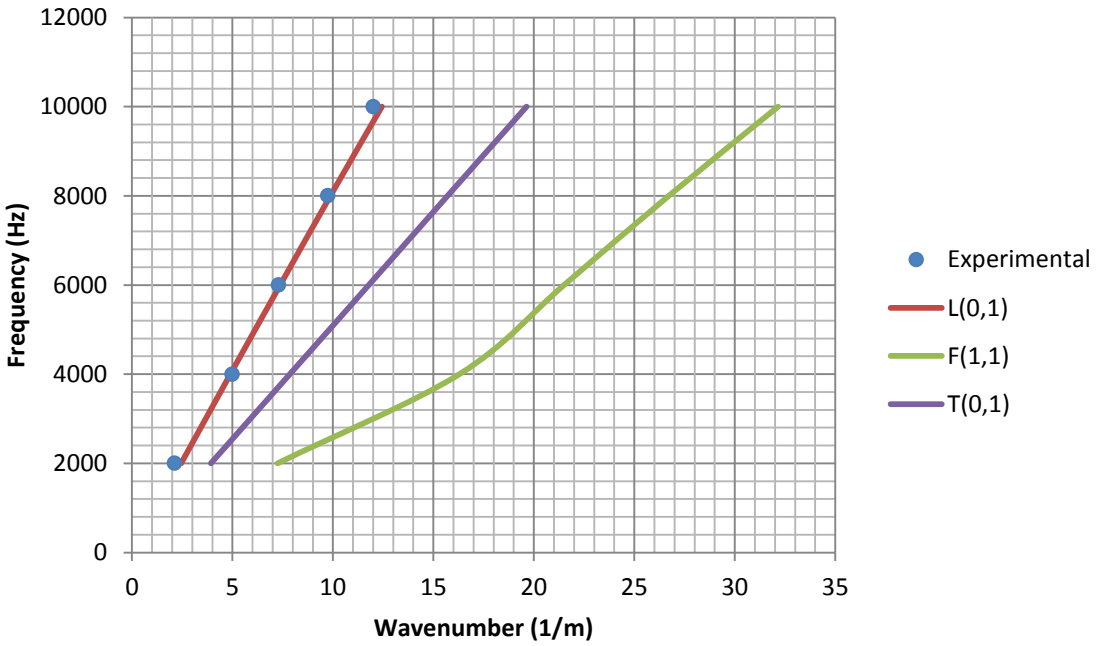

Figure 3.4: Comparison between the experimental and theoretical dispersion curves

CHAPTER IV

THE CONSISTENCY TEST

1. Experimental Setup for the Consistency Test

This test aims at verifying the consistency of the measurements that will be taken in the field. It tries to show that the measurements, the instruments, and the experimental setups are reliable and can be used as a foundation and as a feedback source for a simulation tool. These experiments were carried out in the field using 6 pipe segments, each one nominally 32 feet long and 2 7/8 inches in diameter. The pipe segments were connected to an acoustic transmitter and an accelerometer was used to record those signals. The repeatability of the measurements needed to be tested for three stages: the transmitter, the coupling, and the receiver.

The first set of experiments tried to determine whether the acoustic transmitter can produce repeatable signals. A broadband pulse was transmitted several times and the accelerometer was used to record it. Then, these successive pulses were compared by calculating the correlation coefficients to indicate the level of similarity between them.

The second set of experiments aimed at discovering the best adhesive material that can be used to attach the accelerometer. The accelerometer was attached to the pipe using both glue and wax while the signals coming from the transmitter were recorded several times. These recordings were later compared to determine the similarity between the received signals. The similarity was measured by calculating the correlation coefficients between several recordings as before and the amplitudes were compared as well.

The final set of experiments aimed at discovering which of the orientations of the accelerometer offer reliable measurements and which do not. The accelerometer was attached to the pipe using three different configurations which are the longitudinal (z-direction), the radial (r-direction), and the azimuthal (θ-direction) configurations. Each configuration allows the accelerometer to measure the vibration and the displacements along a certain axis. The orientation of the accelerometer and the direction of the displacements are extremely important for the next Dispersion Test where different modes create displacements in different directions. Figures 4.1-4.3 illustrate these configurations and figures 4.4-4.6 show them in real life.

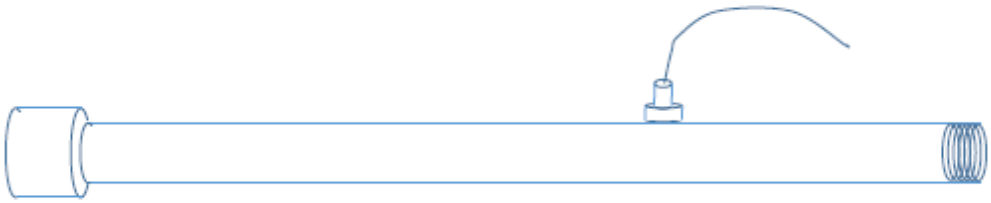

Figure 4.1: R-configuration measurements

Figure 4.2: Z-configuration measurements

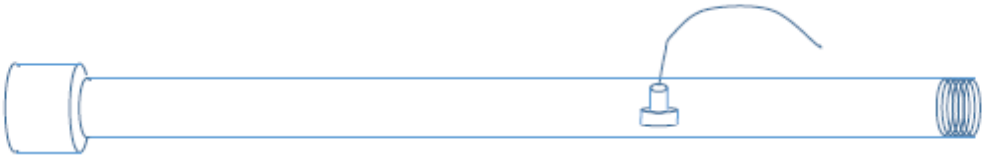

Figure 4.3: θ-configuration measurements

Figure 4.4: Accelerometer r-configuration measurements

Figure 4.5: Accelerometer z-configuration measurements

Figure 4.6: Accelerometer θ-configuration measurements

Several transmitted signals were recorded and the correlation coefficients were calculated between several pairs of recordings in order to determine the consistency of each configuration.

2. Results of the Consistency Test

a. Transmitter Consistency

A total of 6 successive broadband pulses were recorded and the first pulse was used as a reference for comparison with the other pulses. The correlation coefficients were calculated between the first pulse and the remaining ones. Table 4.1 shows the results of this comparison.

Table 4.1: Correlation coefficients for the successive transmitted pulses

Pulses	Pulses 1 and 2	Pulses 1 and 3	Pulses 1 and 4	Pulses 1 and 5	Pulses 1 and 6
Correlation Coefficient	0.9428	0.803	0.9418	0.993	0.9442

Figure 4.7 shows the visual comparison between the 6 successive transmitted pulses where they appear to be in good agreement in terms of both shape and amplitude.

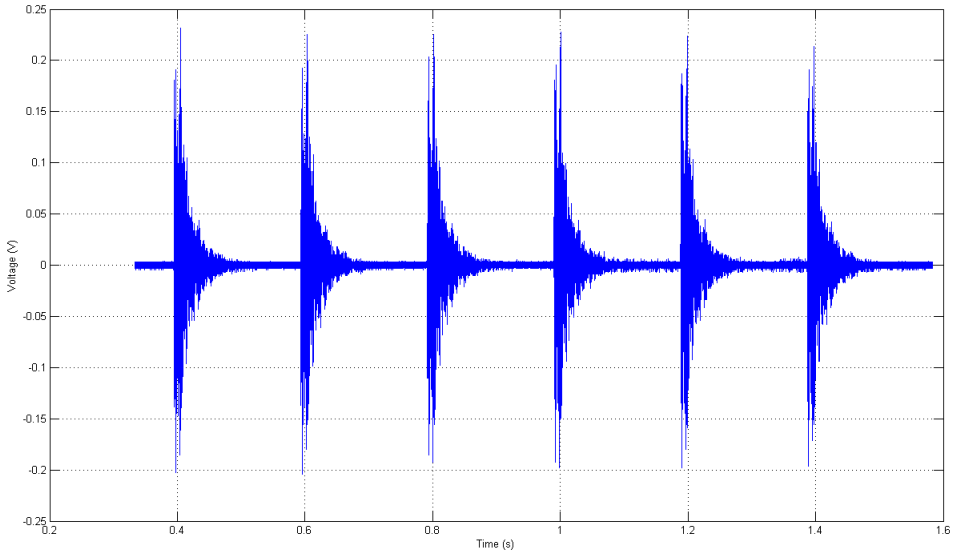

Figure 4.7: Successive transmitted broadband pulses

b. Coupling Consistency

The signals were recorded multiple times for both the r and z directions and the correlation coefficients were calculated for each pair of signals to determine the level of similarity between them. The signals that were transmitted consisted of the default transmitter square waves with linearly increasing frequency. The results are presented in tables 4.2 and 4.3.

Table 4.2: Correlation coefficients for wax measurements

Orientation\ Signal	625-675 Hz Square Wave	1150-1250 Hz Square Wave	225-245 Hz Square Wave	850-900 Hz Square Wave	Broadband Pulse
R-direction	0.8792	0.7883	0.8197	0.9034	0.8323
Z-direction	0.969	0.9547	0.965	0.9694	0.9882

Table 4.3: Correlation coefficients for glue measurements

Orientation\ Signal	625-675 Hz Square Wave	1150-1250 Hz Square Wave	225-245 Hz Square Wave	850-900 Hz Square Wave	Broadband Pulse
R-direction	0.8957	0.6812	0.8229	0.8903	0.8877
Z-direction	0.9712	0.9891	0.9645	0.9615	0.9932

Figures 4.8-4.12 show the transmitted signals that were used as an input for this series of tests. It can be noted from the frequency domain plots that the side lobes for the 625-675 Hz, the 1150-1250 Hz, and the 850-900 Hz are gradually getting wider. This is due to the frequency modulation in the signals. The first series of peaks occur at the transmit frequencies. The next series of peaks represent the harmonics that occur at integer multiples of the transmit frequencies therefore they are spaced further apart than the first series of peaks.

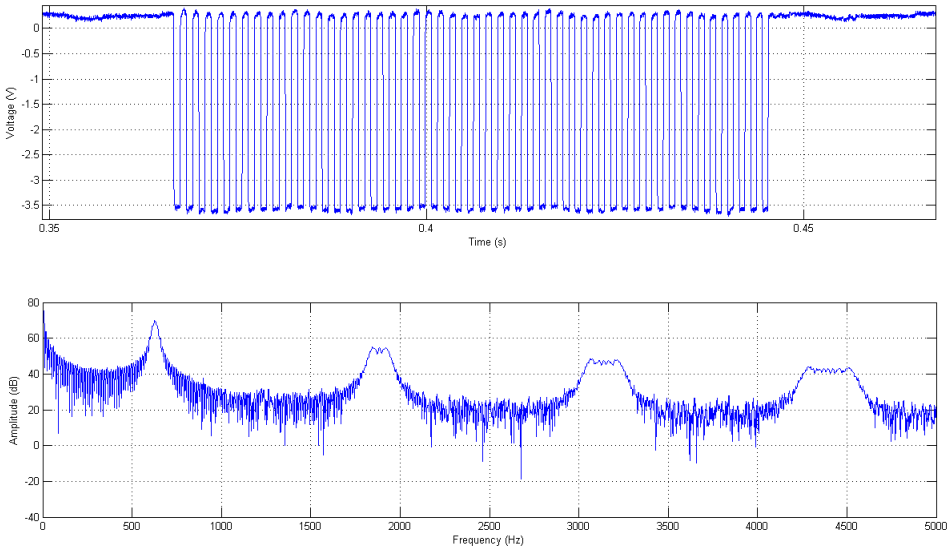

Figure 4.8: 625-675 Hz square wave in time and frequency domains

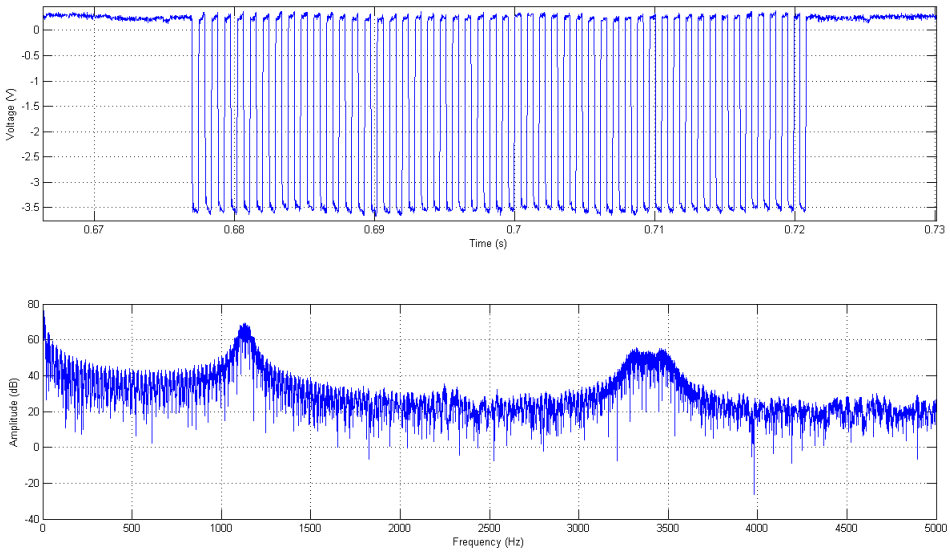

Figure 4.9: 1150-1250 Hz square wave in time and frequency domains

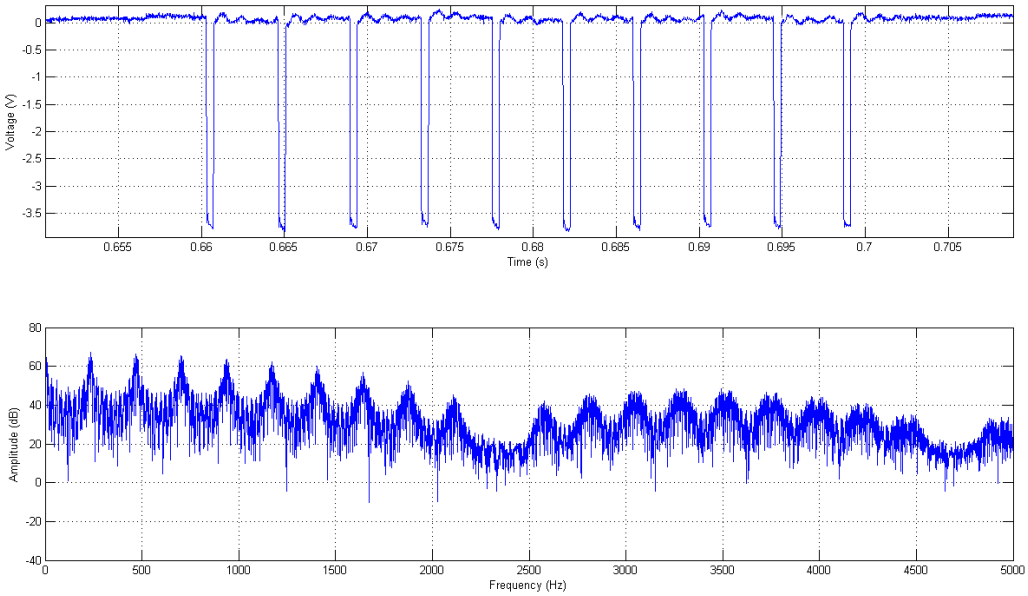

Figure 4.10: 225-245 Hz square wave in time and frequency domains

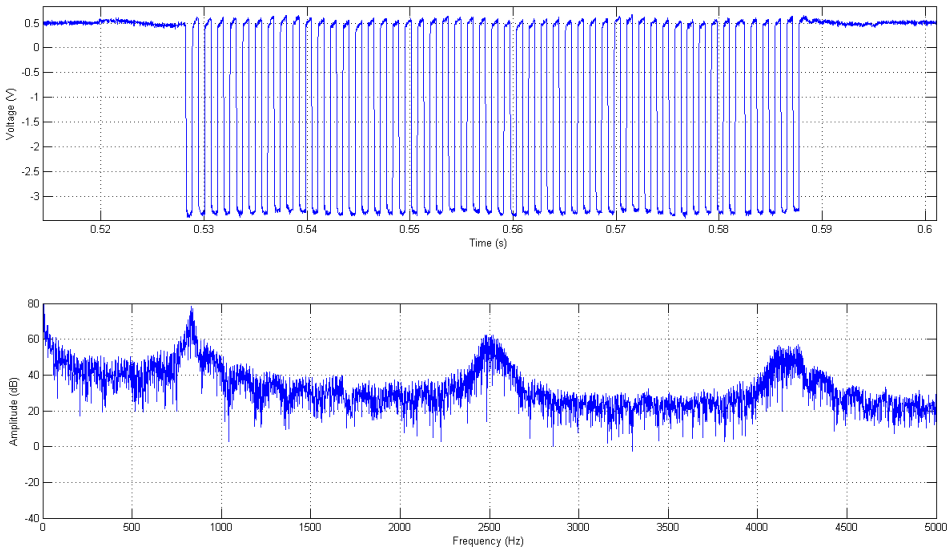

Figure 4.11: 850-900 Hz square wave in time and frequency domains

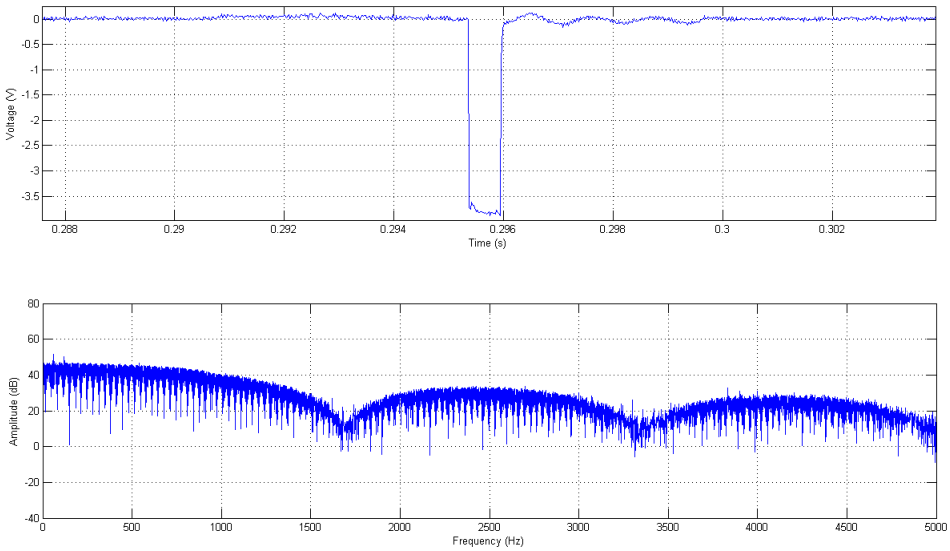

Figure 4.12: Broadband pulse in time and frequency domains

Both materials showed high correlation coefficients that exhibited above 80% similarity most of the time. However, the glue showed a small advantage over the wax and especially for the broadband pulse which was later used as an input to the Dispersion Test.

c. Receiver Consistency

The last set of experiments tried to test the consistency of each measurement orientation for the accelerometer. Two different transmitted signals were sent and in each case the orientation of the accelerometer was alternating between the radial, longitudinal, and azimuthal directions for several measurements. The glue was used to attach the accelerometer and hold it in place. The correlation coefficients were calculated between two pairs of signals for each combination. Tables 4.4 and 4.5 present the findings of this experiment in terms of correlation coefficients and the percentage of relative voltage difference. The percentage of relative voltage difference was calculated by subtracting the two signals for each time sample and taking the average over all samples then dividing the result by the maximum peak value between the two signals.

Table 4.4: Correlation coefficients for the different orientations

Orientation\Signal	850-900 Hz Square Wave	Broadband Pulse
R-direction	0.9579	0.9647
Z-direction	0.9182	0.9141
θ-direction	0.9321	0.8814

Table 4.5: Percentage of relative amplitude difference for the different orientations

Orientation\Signal	850-900 Hz Square Wave	Broadband Pulse
R-direction	% 14.98	% 2.69
Z-direction	% 12.74	% 2.61
θ-direction	% 7.752	% 2.5

Table 4.4 shows that all three orientations presented consistent data that exceeded 90% similarity in most cases. Table 4.5 shows that the percentage of relative difference in amplitude between the compared signals is much better for the broadband pulse. Therefore, the broadband pulse produced better consistency in terms of shape and amplitude of the signals. As a result, the broadband pulse was later used for the Dispersion Test. Figures 4.13-4.18 show the visual comparison between the different combinations of measurements.

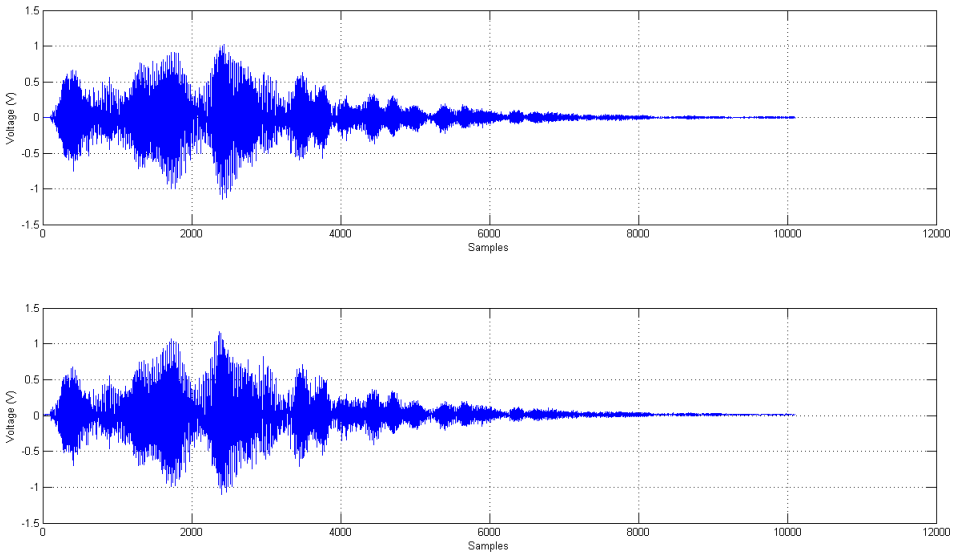

Figure 4.13: 850-900 Hz square wave measured in the radial direction

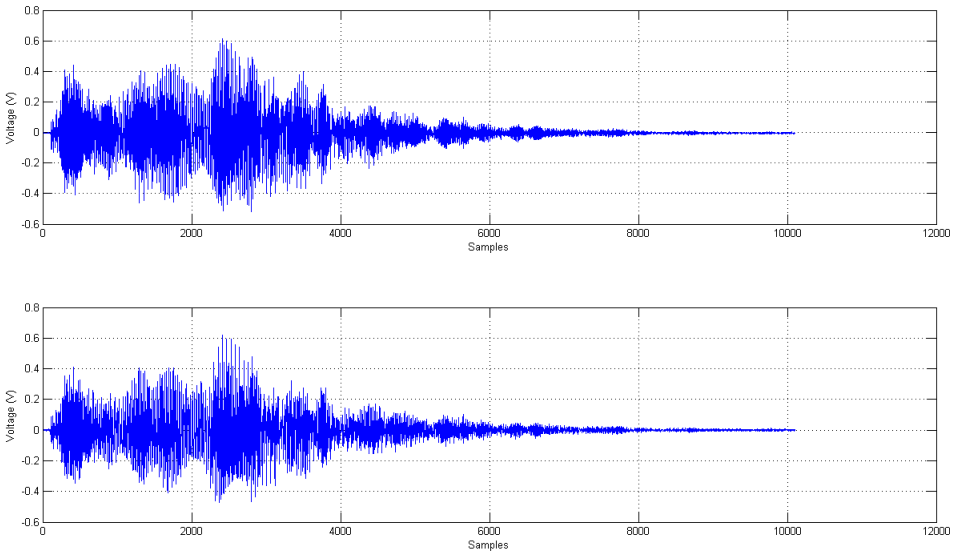

Figure 4.14: 850-900 Hz square wave measured in the azimuthal direction

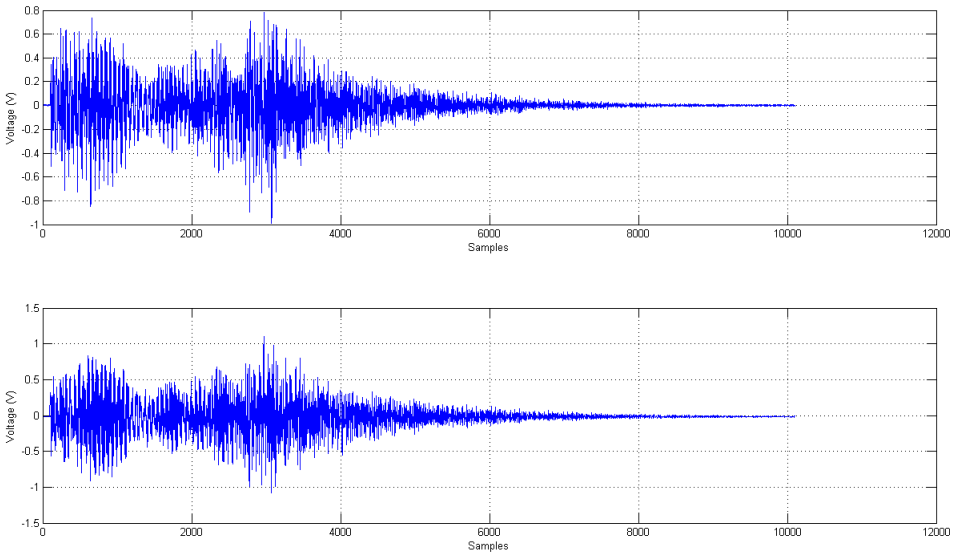

Figure 4.15: 850-900 Hz square wave measured in the longitudinal direction

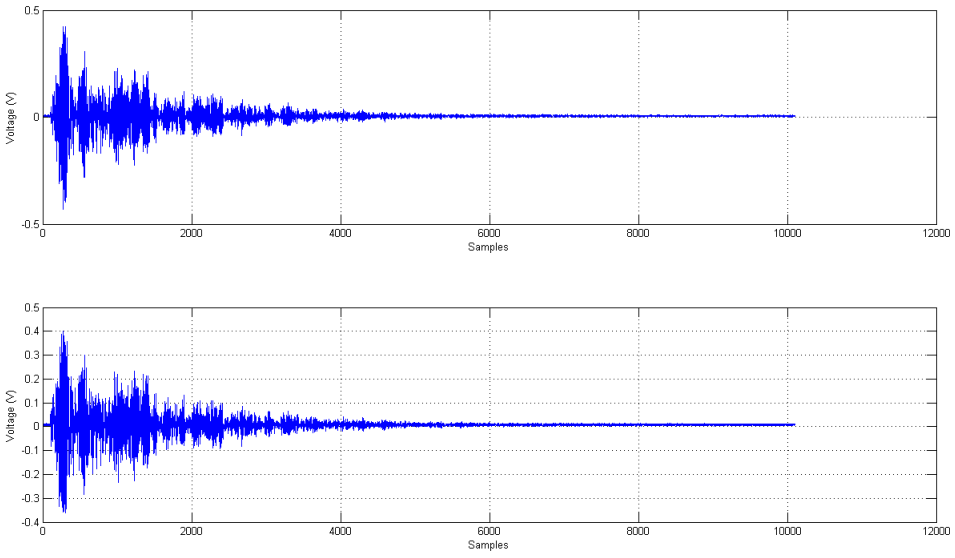

Figure 4.16: Broadband pulse measured in the radial direction

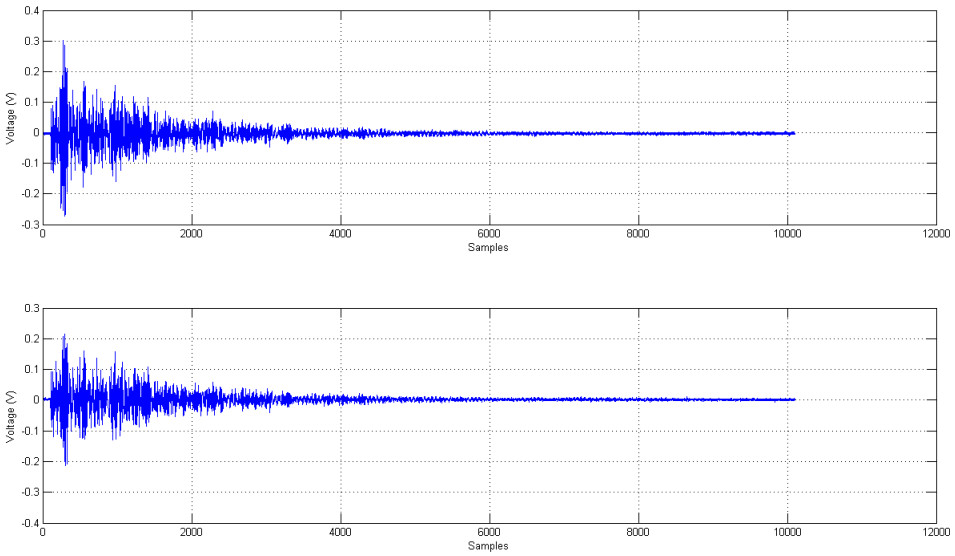

Figure 4.17: Broadband pulse measured in the azimuthal direction

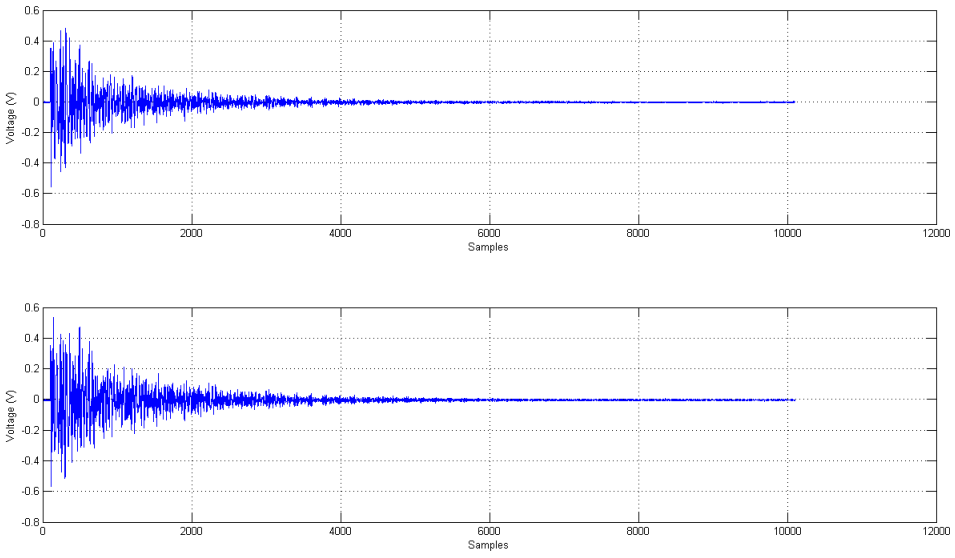

Figure 4.18: Broadband pulse measured in the longitudinal direction

CHAPTER V

THE DISPERSION TEST

1. Experimental Setup for the Dispersion Test

Once the previous two experiments are successful, this test consists of measuring a transmitted signal in several locations in order to produce an experimental dispersion curve and determine whether it matches the theoretical dispersion curves and whether all of the predicted vibrational modes are present.

An experimental dispersion curve can be produced by two possible means. The first method was used during the Existence Test where signals with different center frequencies are allowed to propagate a certain known distance and then recorded at the receiver. The propagation delay is then estimated and the phase velocity can be calculated as in equation (3.1). From there, the wavenumber can be calculated from equation (3.2) and the frequency-wavenumber pair is found. The second method involves a more complicated setup but produces more reliable data. It consists of measuring the transmitted signal at a series of equidistant positions and arranging the data in an array where each column represents a signal measured in time at a certain location. Then a two-dimensional Fourier Transform is carried out in the following manner [33, 34]. First compute the temporal Fourier Transform over each column to obtain the frequency spectrum for each position then compute a spatial Fourier

Transform over each row to obtain the frequency-wavenumber information and thus producing a dispersion curve. The output of the 2D-FFT is related to the data $u(x,t)$ by equation (5.1).

$$H(k,f) = \int_{-\infty}^{+\infty} \int_{-\infty}^{+\infty} u(x,t) e^{-i(kx+\omega t)} dx dt \tag{5.1}$$

Figure 5.1 shows the experimental setup that was used to perform the Dispersion Test.

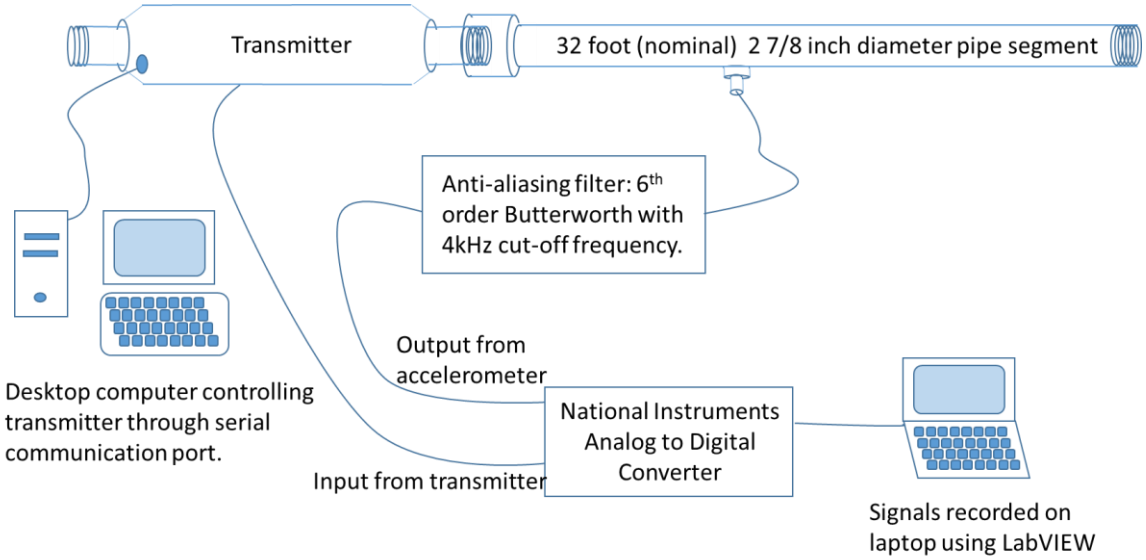

Figure 5.1: Experimental setup for the Dispersion Test

A broadband pulse was sent from the transmitter and was recorded in the 1st, 3rd, and 5th pipe segments using the accelerometer that was placed in both the z-direction to capture the longitudinal L(0,1) mode and in the θ-direction to capture the flexural F(1,1) mode

and the torsional T(0,1) mode. For each pipe segment, the signal was recorded starting at 8 feet from the beginning in 32 different positions that were separated by 6 inches. Figure 5.2 shows the pipe segments and the measurement locations.

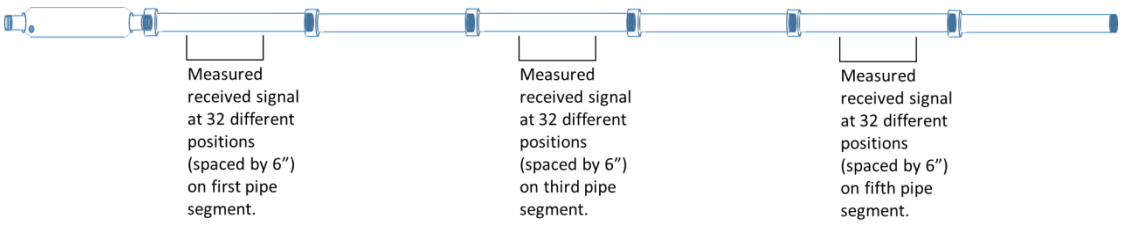

Figure 5.2: Pipe segments and measurement locations for the Dispersion Test

The joints were each 5.25 inches long and the 6 pipe segments used in the experiment had varying lengths that are summarized in Table 5.1. The outer diameter was 3.5 inches and the thickness of the pipes was 0.25 inches.

Table 5.1: Lengths of the pipe segments used in the Dispersion Test

Pipe Segment	Length (feet)
1	32.323
2	32.24
3	32.266
4	32.208
5	32.302
6	32.385

The transmitter is an instrument that only takes digital waveforms as input and sends acoustic signals according to that input. However, the impulse response of the transmitter is unknown. Thus, it is not possible to predict the shape of the transmitted signal and they can only be viewed at the receiving end. This ambiguity however does not affect the success of the Dispersion Test since the frequency content is the only required information about the signal in order to produce a dispersion curve. Besides, the transmitter is still able to produce both broadband and narrowband signals at any desired frequency in the acoustic range.

The transmitted signal was a broadband pulse that was recorded in order to have a time reference so that the appropriate propagation delay can be measured and accounted for in

each received signal before they are placed in an array as a preparation to the 2D-FFT procedure.

In addition, a 6th order low-pass Butterworth filter with cutoff frequency at 4 kHz was used as an anti-aliasing filter to limit the bandwidth of the broadband pulse. The filter was designed by a cascade of three 2nd order low-pass filters built using the Sallen-Key topology as shown in Figure 5.3. An NI USB-6009 analog to digital converter sampling at 24 kHz was used to convert the data and read it in LabVIEW and later in MATLAB.

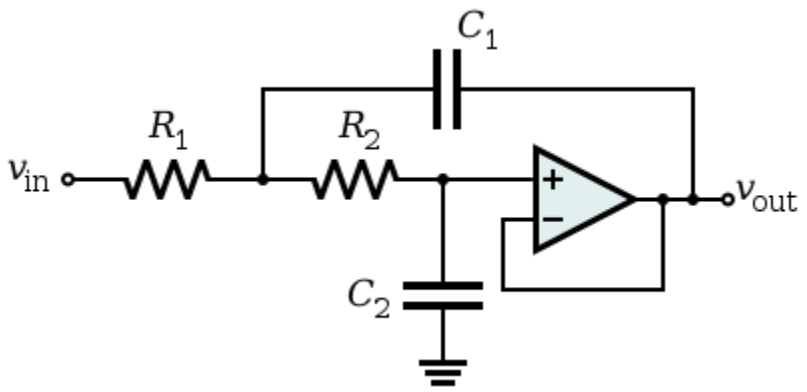

Figure 5.3: 2nd order Sallen-Key low-pass filter

The poles of the designed filter needed to match those of the theoretical 6th order Butterworth low-pass filter. The filter needed to have a flat magnitude and phase responses in the passband and constant phase and group delays. Figures 5.4-5.6 describe the behavior of the anti-aliasing filter designed to limit the bandwidth of the signals and Table 5.2 shows the component values chosen for the design of each stage. The phase

and group delays peak at the cutoff frequency due to the sudden change in the frequency response of the filter.

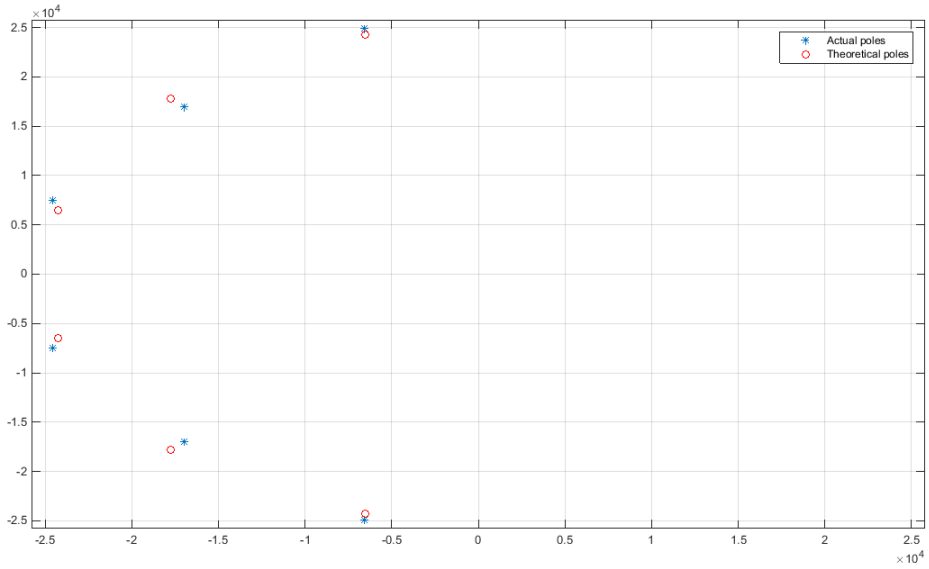

Figure 5.4: Comparison between the poles of the designed filter and the theoretical poles

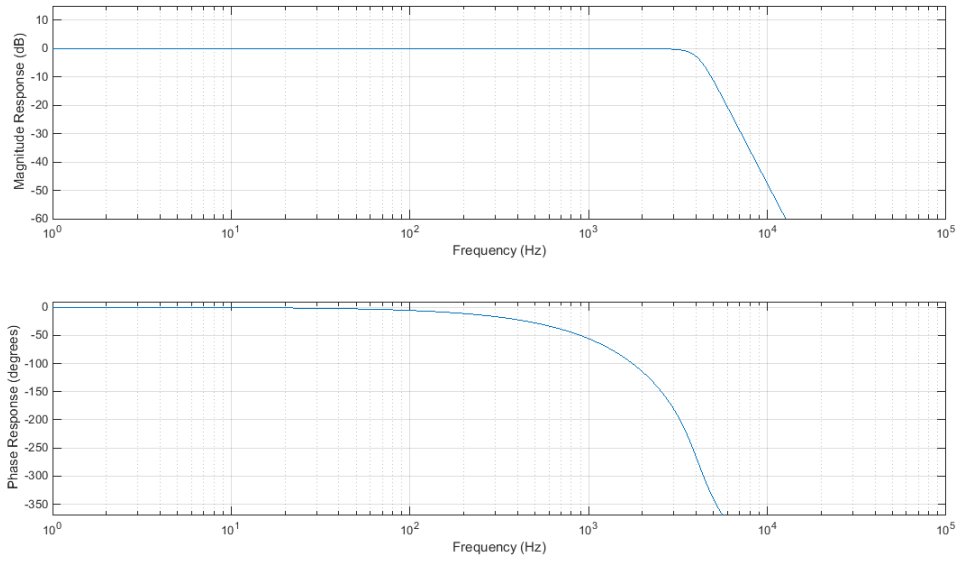

Figure 5.5: Magnitude and phase responses of the anti-aliasing filter

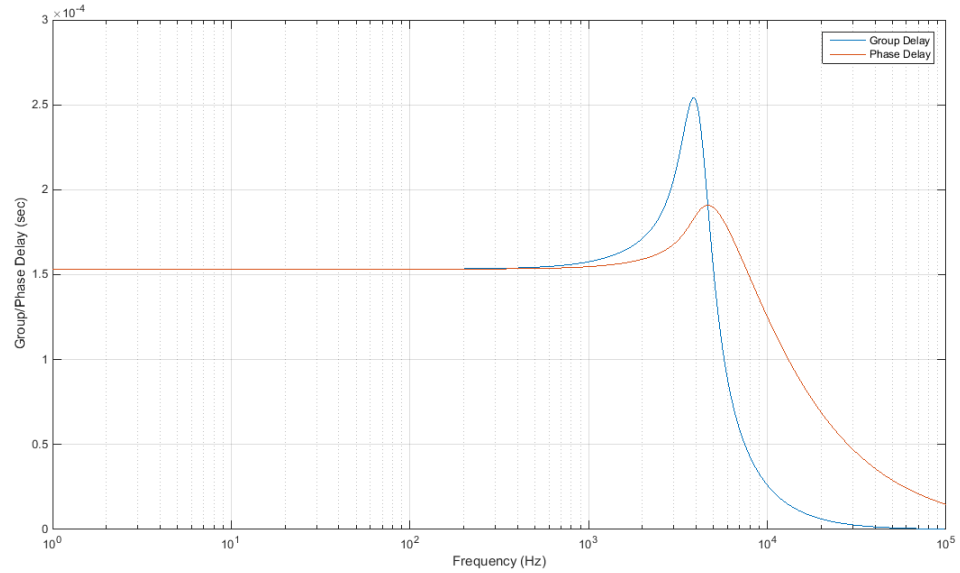

Figure 5.6: Group delay and phase delay of the anti-aliasing filter

Table 5.2: Component values for the anti-aliasing filter

Stages\Component Values	$R_1(\Omega)$	$R_2(\Omega)$	$C_1(nF)$	$C_2(nF)$
1st Stage	2280	510	47	22
2nd Stage	1680	1000	47	22
3rd Stage	3200	1000	100	4.7

2. Results of the Dispersion Test

Figures 5.7-5.12 show the comparison between the experimental dispersion curves generated using the 2D-FFT of the measured data and the theoretical dispersion curves generated using the PCDISP program [29, 31]. The colors indicate the amplitude of the output of the Fourier Transform in decibels. Warm colors indicate high amplitudes and cold colors indicate low amplitudes. The peaks of the curves correspond to the frequencies and the wavenumbers at which the acoustic wave was propagating.

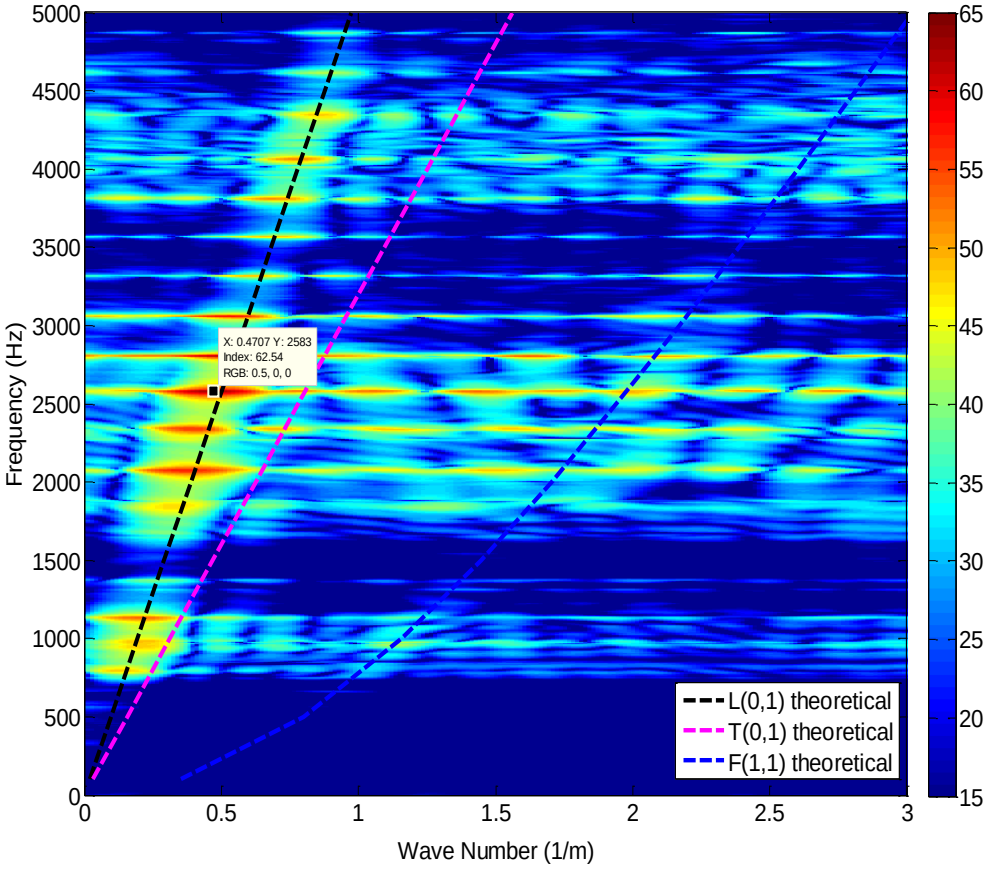

Figure 5.7: Comparison of theoretical and experimental dispersion curves for the 1st pipe segment in the z-direction

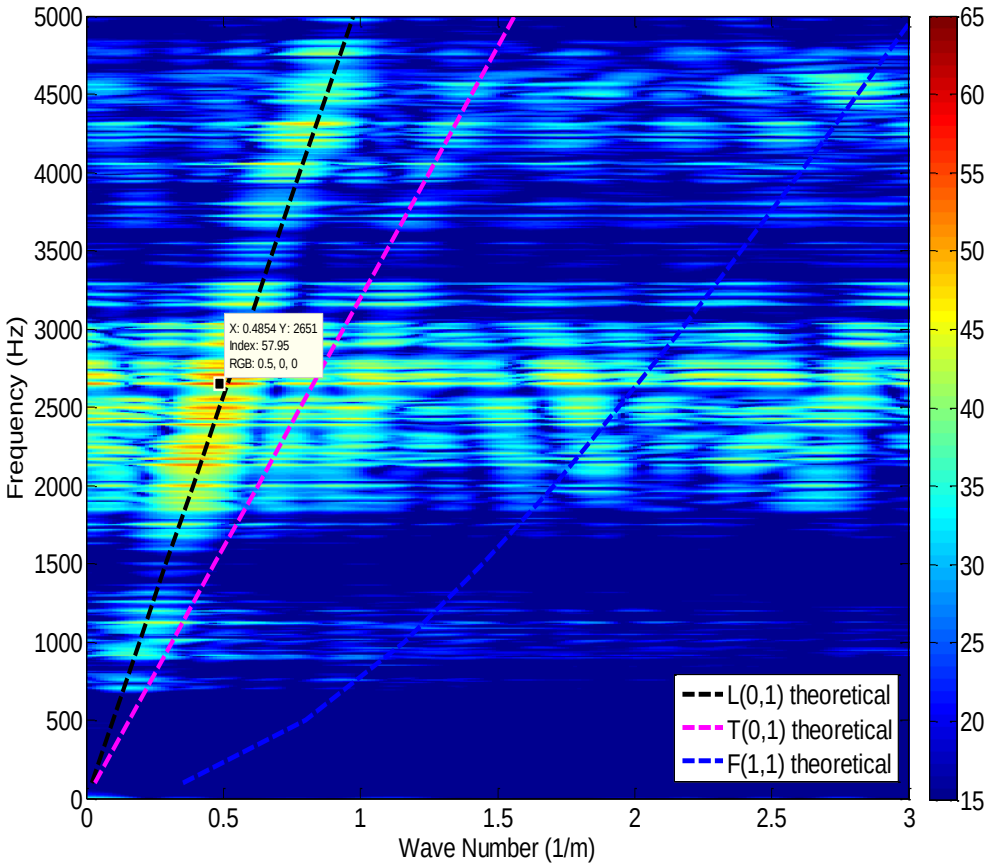

Figure 5.8: Comparison of theoretical and experimental dispersion curves for the 3rd pipe segment in the z-direction

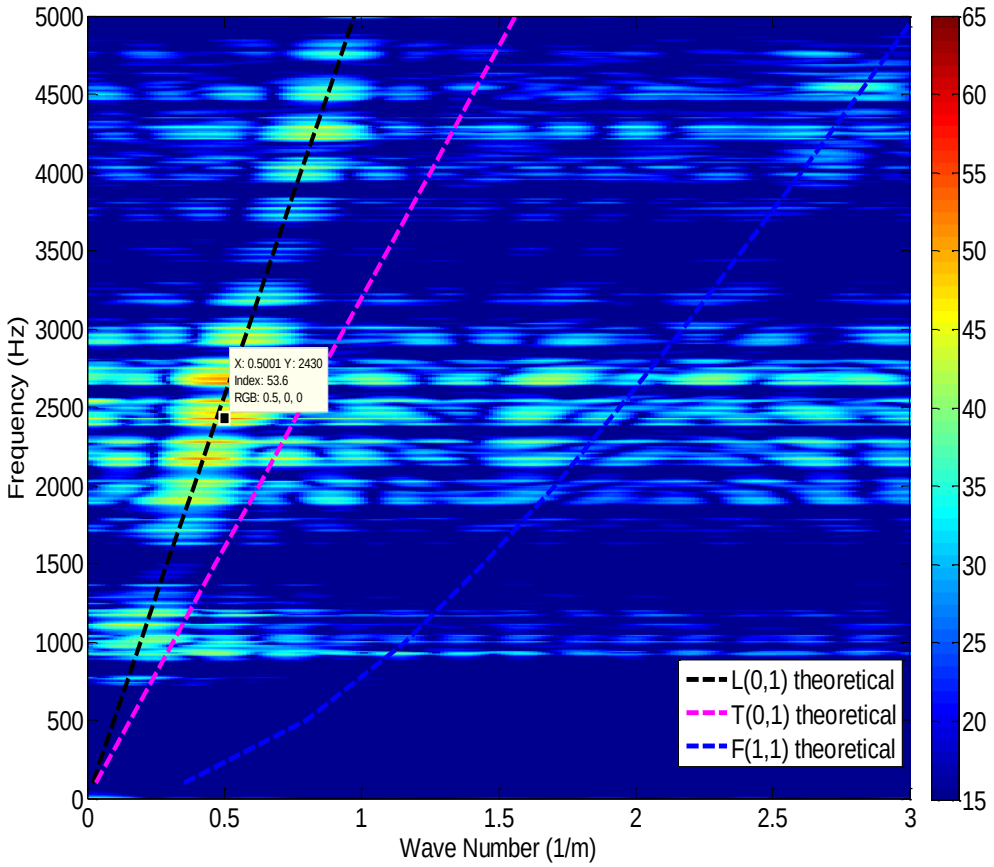

Figure 5.9: Comparison of theoretical and experimental dispersion curves for the 5th pipe segment in the z-direction

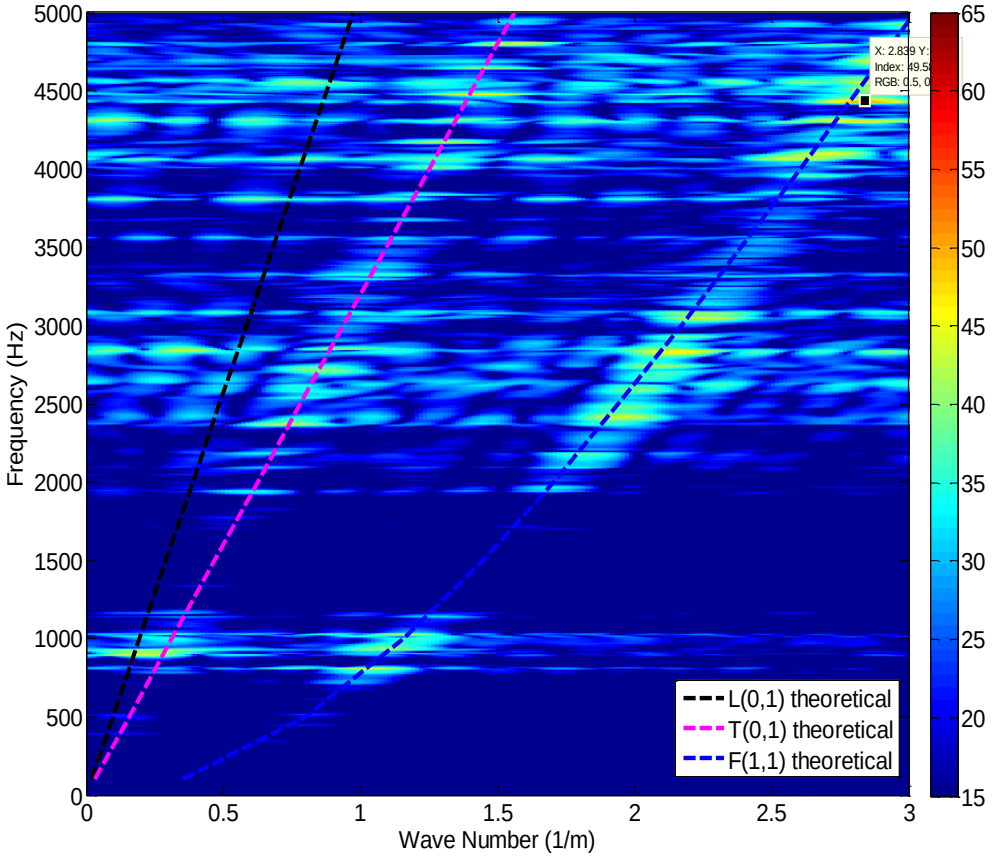

Figure 5.10: Comparison of theoretical and experimental dispersion curves for the 1st pipe segment in the θ-direction

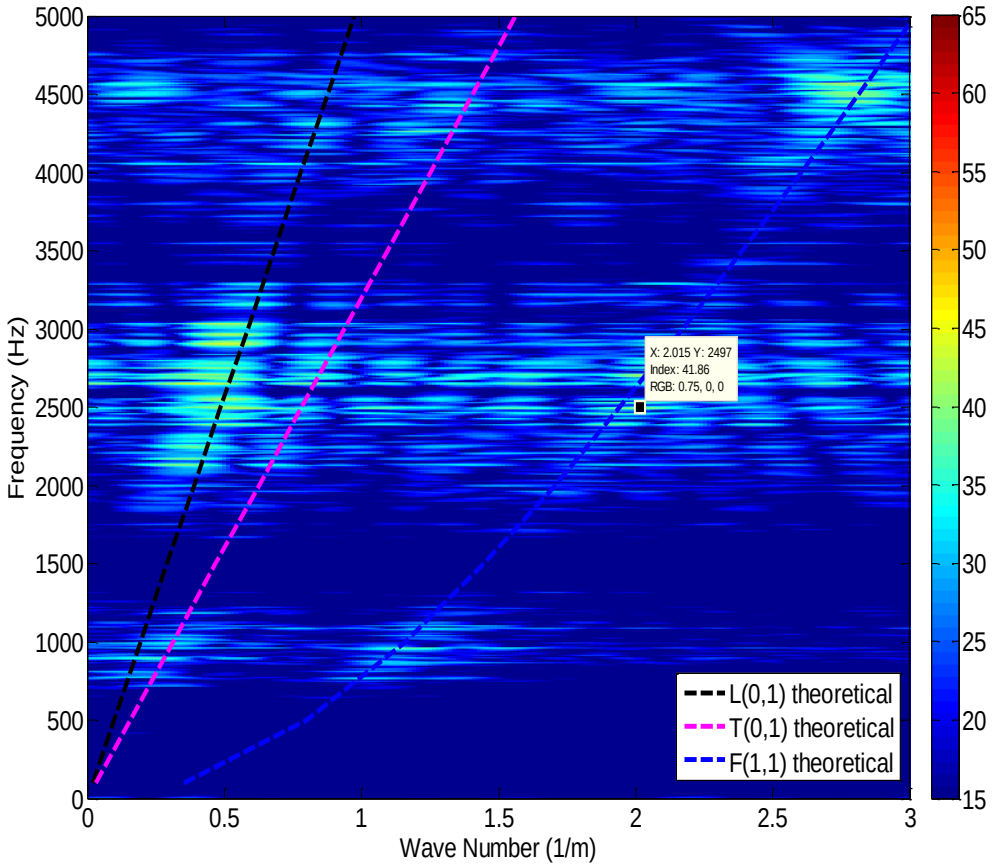

Figure 5.11: Comparison of theoretical and experimental dispersion curves for the 3rd pipe segment in the θ-direction

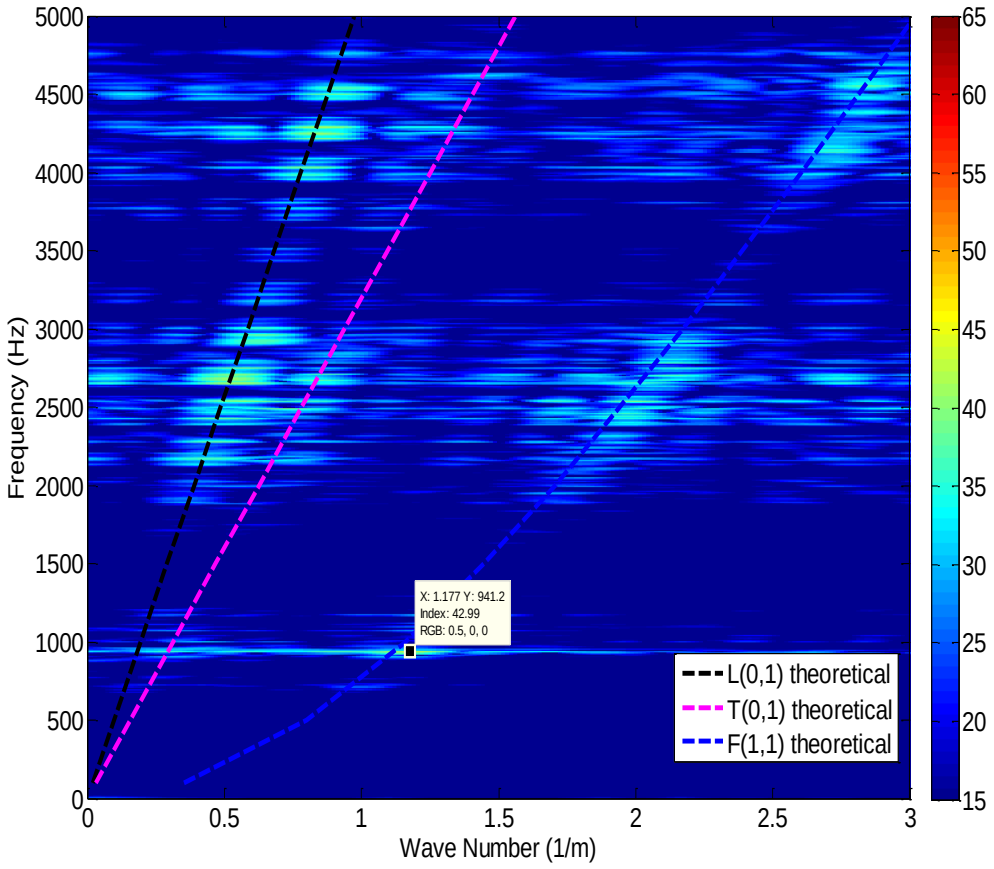

Figure 5.12: Comparison of theoretical and experimental dispersion curves for the 5th pipe segment in the θ-direction

After careful observation of figures 5.7-5.12, one can observe that the theoretical curves and the experimental curves are matching well.

Due to the presence of unwanted frequency content, some of the weaker modes were not clearly seen. Therefore, further processing was required. In order to improve the plots, each row in the resulting two-dimensional Fourier Transform was divided by its maximum value. Thus, the amplitudes were normalized and the disturbance that

occurred in the previous plot was minimized. Figures 5.13 and 5.14 show the dispersion curves after normalization.

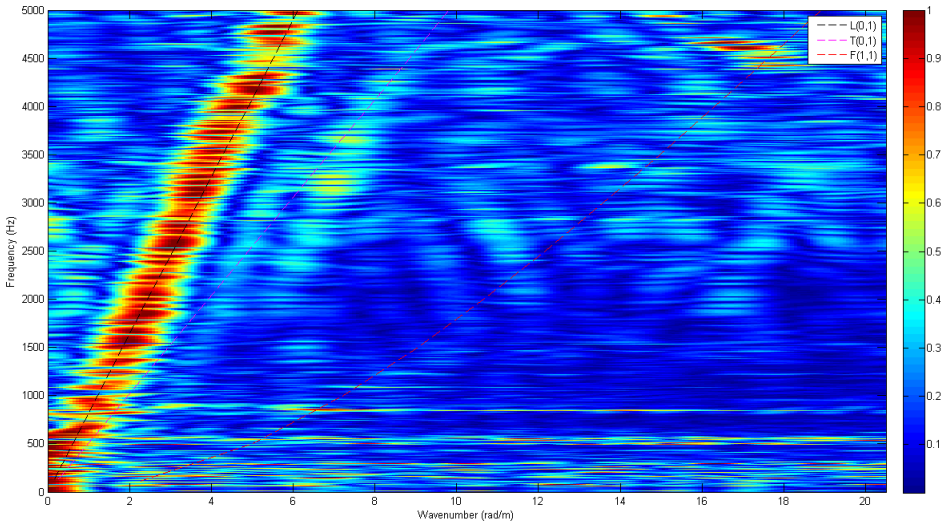

Figure 5.13: Normalized experimental dispersion curve in the z-direction showing the L(0,1) mode

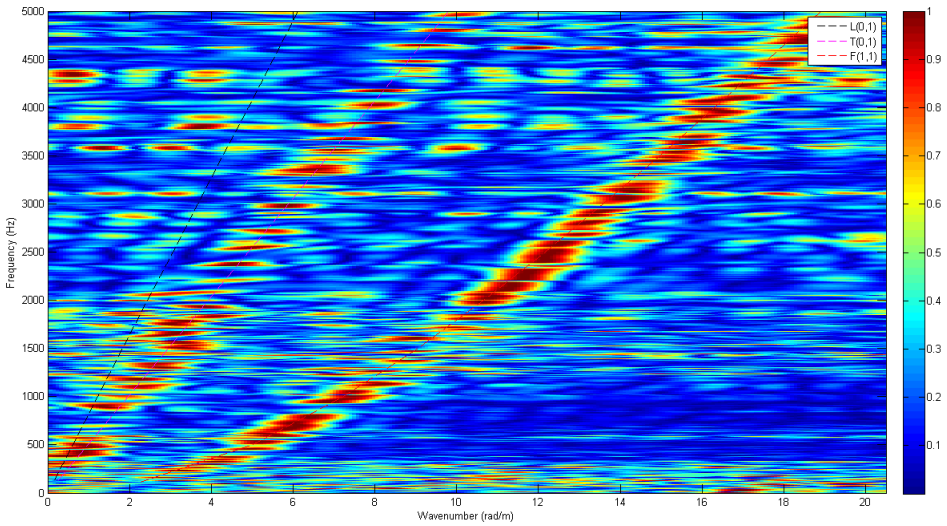

Figure 5.14: Normalized experimental dispersion curve in the θ-direction showing the F(1,1) and the T(0,1) modes

CHAPTER VI

THE FREQUENCY TEST

1. Experimental Setup for the Frequency Test

The goal of this experiment is to explore how narrowband signals with different frequencies and broadband signals propagate in the pipe strings and how the energy in the signals decays as a function of distance. This test helps to characterize the frequency response of the pipe strings.

A sequence of narrow band tone bursts lasting each 50ms and covering a range of frequencies from 100 Hz to 3000 Hz with a step size of 100 Hz were transmitted using the transmitter and the acoustic wave was recorded in 6 different positions located at 1 foot after the beginning of each pipe segment with the accelerometer placed in the z-direction. Figure 6.1 illustrates the measurement points for the Frequency Test.

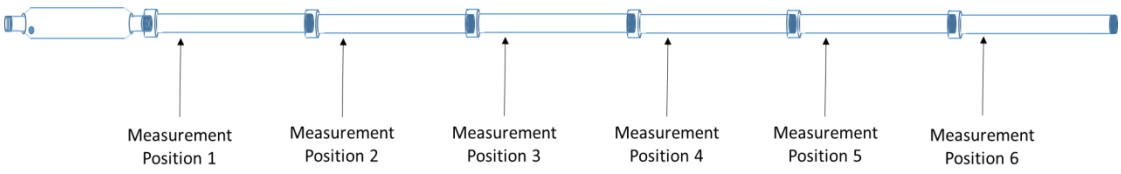

Figure 6.1: Pipe segments and measurement locations for the Frequency Test

The transmitter created a large number of undesirable harmonics that needed to be filtered out later in MATLAB using an 8^{th} order Butterworth low-pass filter with different cutoff frequencies depending on the frequency of the generated tone burst.

A second series of tests was performed in order to verify the existence of passbands and stopbands in the pipe strings. It consisted of transmitting a series of broadband pulses and then making the measurements at different locations. The data for this test was gathered during the Dispersion Test which consisted of sending a broadband pulse and recording it at 32 different locations for three pipe segments. The measurements for the 3^{rd} and 5^{th} pipe segments were performed with all six pipe segments connected while the measurements for the 1^{st} pipe segment were performed with the 1^{st} pipe segment connected. This was done in order to verify the results of Drumheller in [9] about the effect of the number of pipe segments on the passbands and stopbands.

2. Results of the Frequency Test

a. Time Domain Observations

The recorded signals in the time domain can be split in three components: the main pulse that arrives first, followed by large and equally spaced reflections coming from the far end of the pipe strings, and smaller reflections that are not equally spaced caused by the presence of joints between the different pipe strings.

After careful observation of the time domain plots, one can come to a series of conclusions:

- The main reflections coming from the far end of the pipe arrive at equally spaced time intervals as shown in Figure 6.2.
- The weaker reflections coming from the joints appear at inconsistent time intervals due to the fact that the pipe segments do not have the same lengths. Therefore, the measurement points will not be at the same position with respect to the joints.
- The weaker reflections coming from the joints arrive much faster than the main reflections since they propagate smaller distances. They appear between the main pulse and the first large reflection and between every two large reflections. As a result, they merge and accumulate then add up to one of the large reflections causing it to exceed the others in terms of amplitude. However, they can also add destructively and weaken the received signal if they collide and their amplitudes are opposites of each other. This is shown in Figure 6.2.

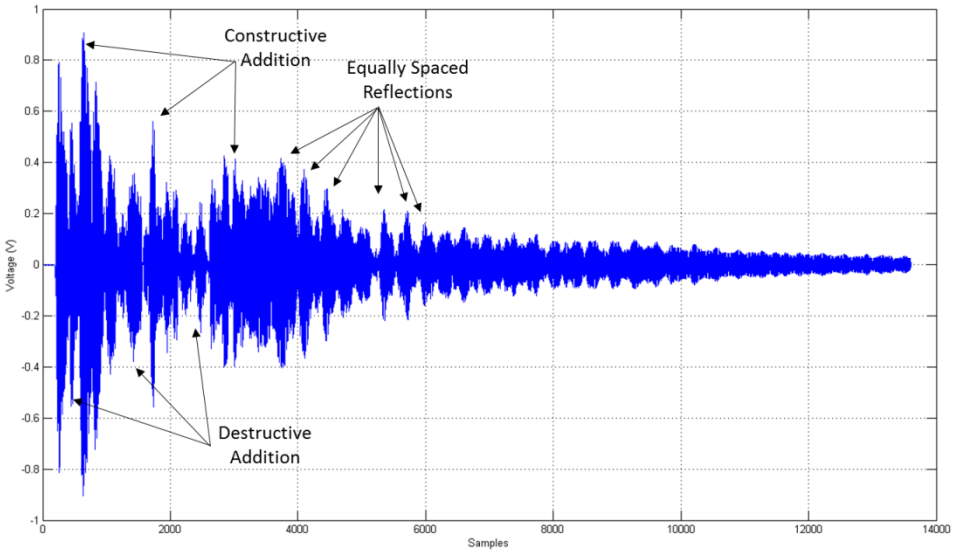

Figure 6.2: 2800 Hz pulse measured at position 5

b. Frequency Domain Observations

The observation of the frequency content of the received signals showed that the transmitter successfully transmitted narrowband signals at different frequencies and that the pipe strings acting as a wireless channel allowed the successful transmission of all desired pulses. In addition, the low-pass filters applied later were successful in attenuating the harmonics and keeping their frequency content around 40 dB below the main transmit frequency. Figures 6.4-6.8 show the frequency content for selected frequencies from the transmitted pulses between 100-3000 Hz pulses.

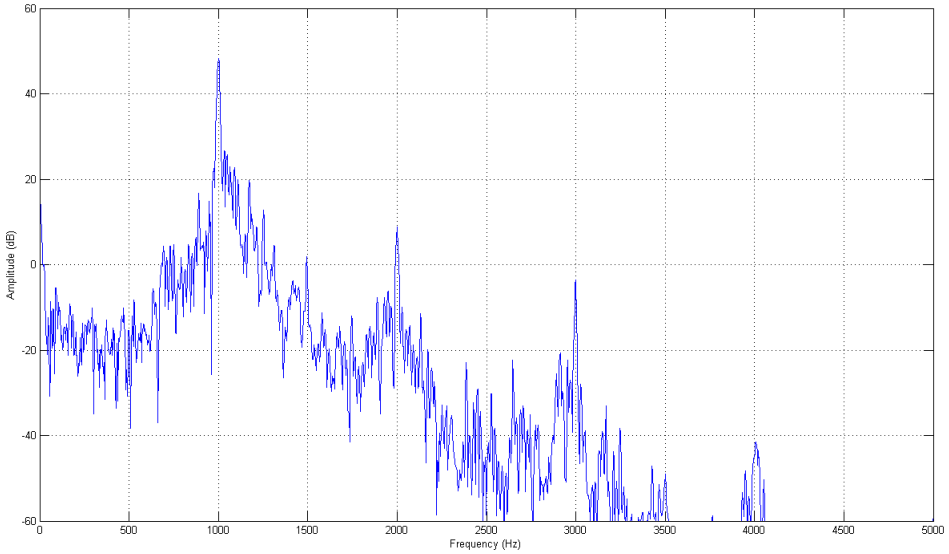

Figure 6.3: Frequency content of the 1000 Hz pulse

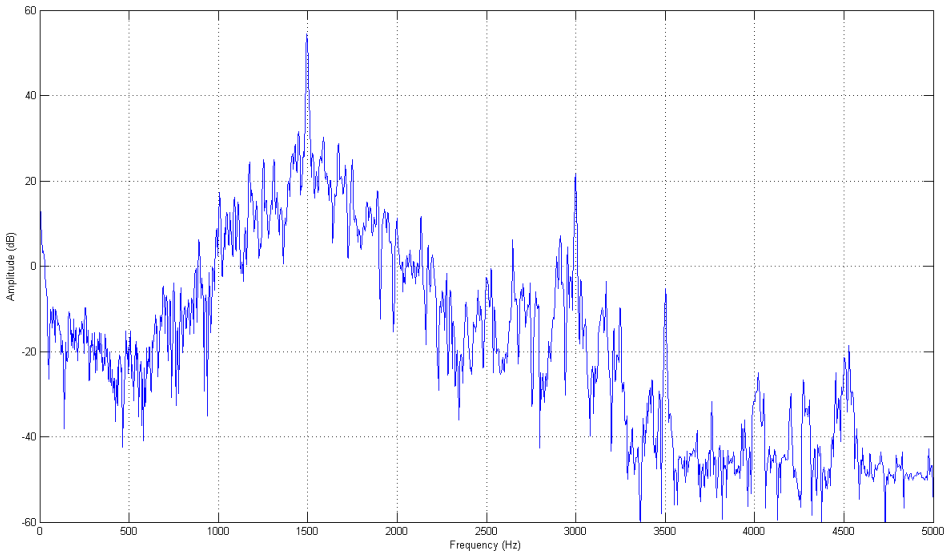

Figure 6.4: Frequency content of the 1500 Hz pulse

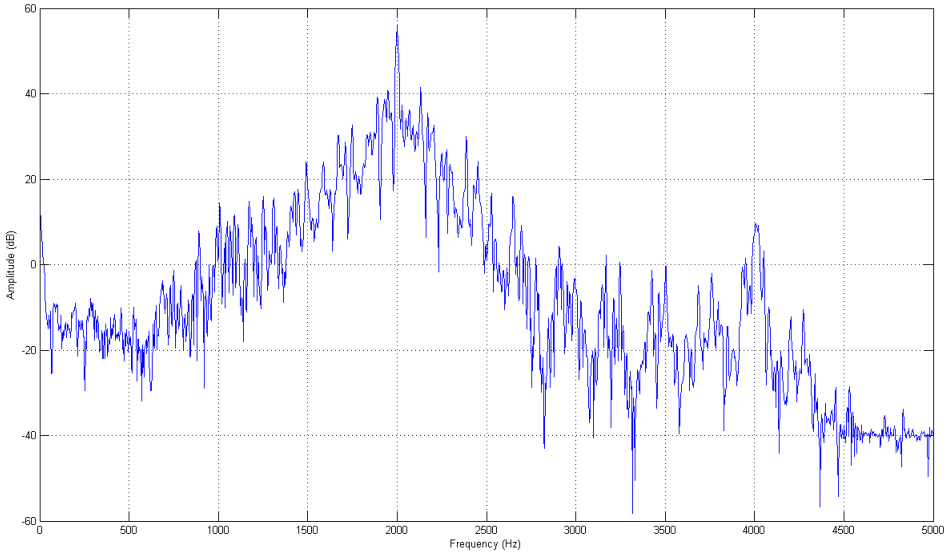

Figure 6.5: Frequency content of the 2000 Hz pulse

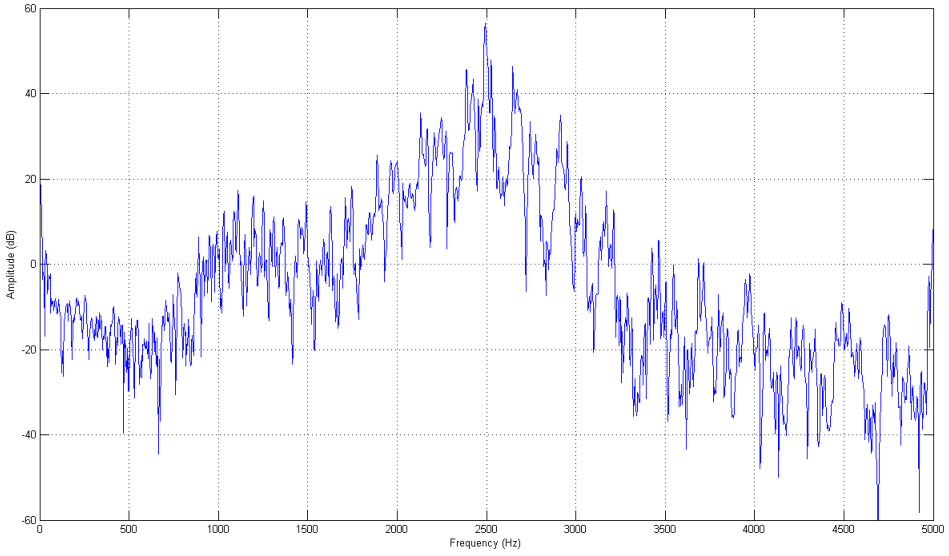

Figure 6.6: Frequency content of the 2500 Hz pulse

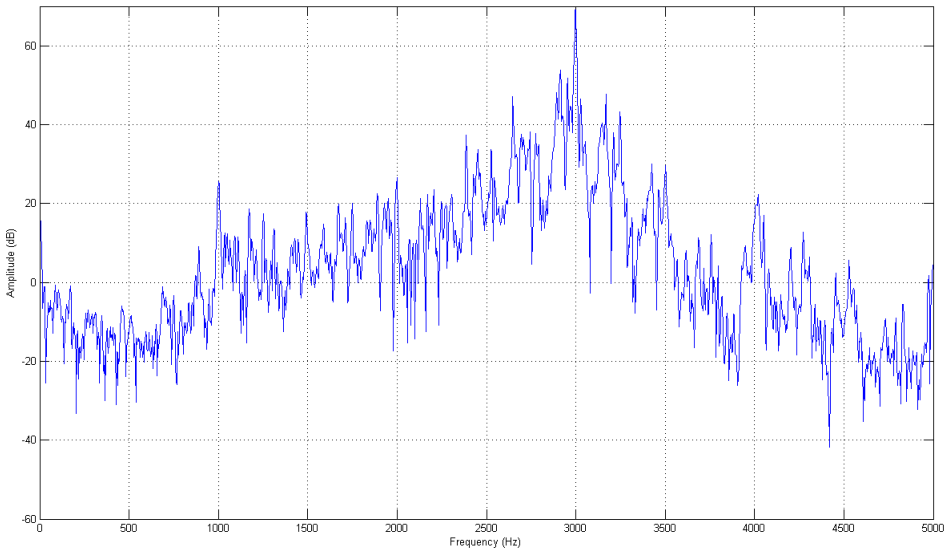

Figure 6.7: Frequency content of the 3000 Hz pulse

c. Passbands and Stopbands Observations

Examination of the data gathered during the Dispersion Test proved the existence of passbands and stopbands in the pipe strings. Figures 6.8-6.10 show a comparison of the frequency content for the measurements performed on the three pipe segments at positions 10, 20, and 30 of the Dispersion Test which were respectively at 12.5 feet, 17.5 feet, and 22.5 feet from the beginning of each pipe segment.

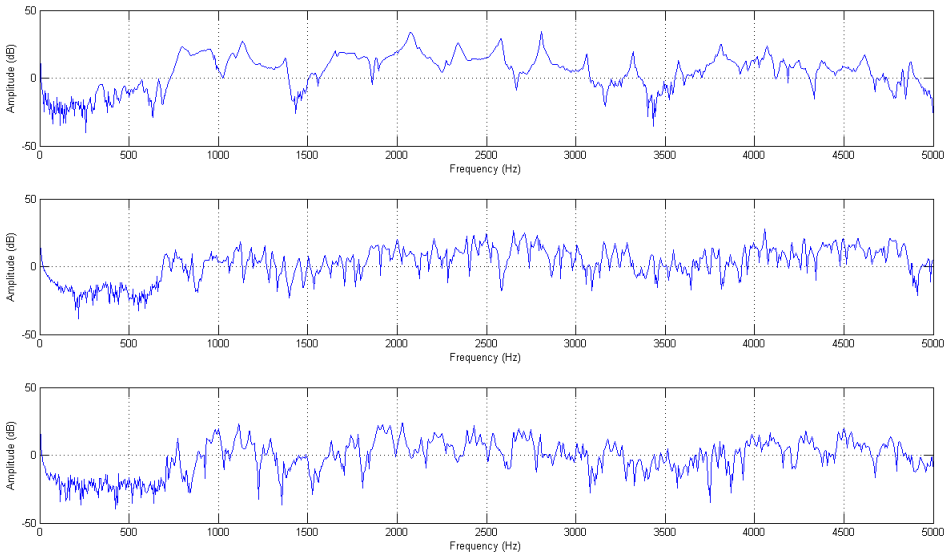

Figure 6.8: Passbands and stopbands for the 1st (top), 3rd (middle), and 5th (bottom) pipe segments at position 10 (12.5 feet from the beginning of the segment)

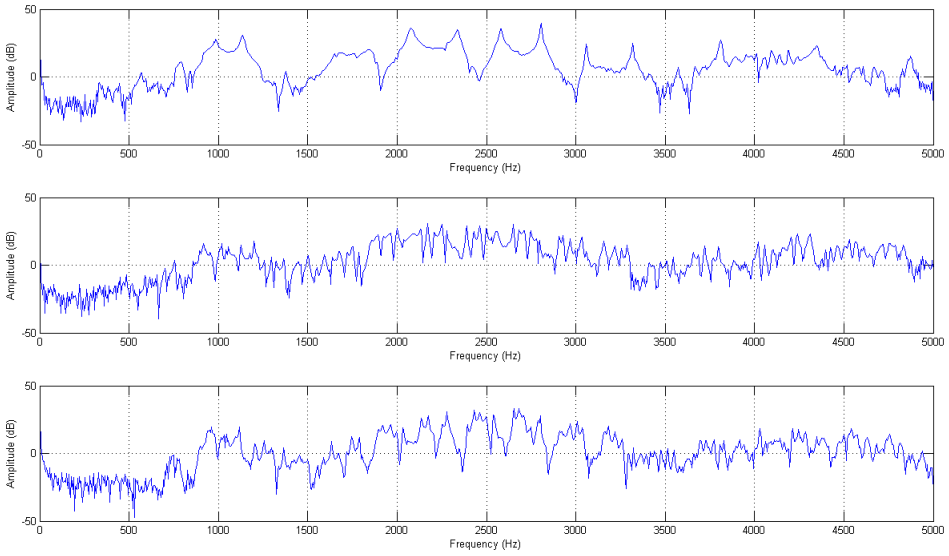

Figure 6.9: Passbands and stopbands for the 1st (top), 3rd (middle), and 5th (bottom) pipe segments at position 20 (17.5 feet from the beginning of the segment)

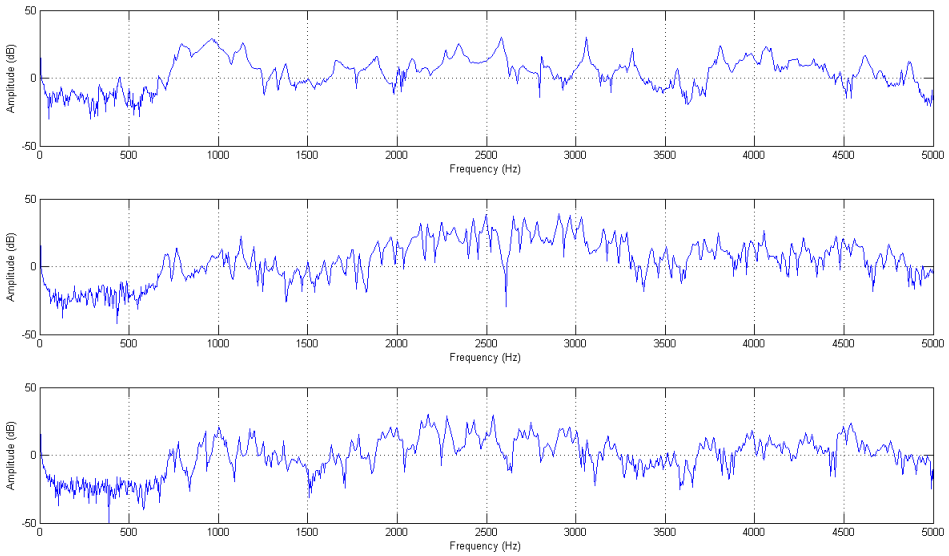

Figure 6.10: Passbands and stopbands for the 1st (top), 3rd (middle), and 5th (bottom) pipe segments at position 30 (22.5 feet from the beginning of the segment)

After careful examination of the above plots, it can be observed that there exist several stopbands and passbands which meant that different frequency components of the signal are affected differently. In other words, several frequencies are getting attenuated while others are getting amplified. The stopbands and passbands are illustrated by the several dips and spikes in Figures 6.8-6.10. The reason behind this is that for a given frequency, the wavenumbers can be either real or complex. When the wavenumber is real, the frequency corresponding to that number appears in the passband of the pipe strings and when the wavenumber is complex, its corresponding frequency appears in the stopband [9].

In terms of propagating distance, the passbands and stopbands appear at roughly the same frequencies for each pipe segment. For the middle and bottom plots in figures 6.8-6.10, it can be noted that the dips and spikes are roughly aligned and occur at the same frequencies. This is expected since there two measurements were performed with all six pipe segments present during the experiment. However, for the top plots in figures 6.8-6.10, the passbands and stopbands appear to be less in terms of number. This is due to the presence of the extra pipe segments for the measurements taken at the 3rd and 5th segments. If there are n pipe strings, it is expected to see n spikes in the passband. The reason behind this phenomenon is that each of the n pipe segments requires a change in frequency in order to fit an extra half of the wavelength, since the pipe is dispersive, causing a resonance at these frequencies demonstrated by the spikes [9].

Figure 6.11 compares the passband between 900 Hz and 1200 Hz for the measurements at the 1st and 3rd pipe segments. It shows that there exists what looks like six highlighted spikes roughly spaced by 50 Hz when the six pipe segments are present while there are no significant spikes when only one segment is connected. There still appears to be some distortion due to noise and experimental error. For the purpose of demonstration, a band-pass filter was utilized to filter out the frequency content below 900 Hz and above 1200 Hz.

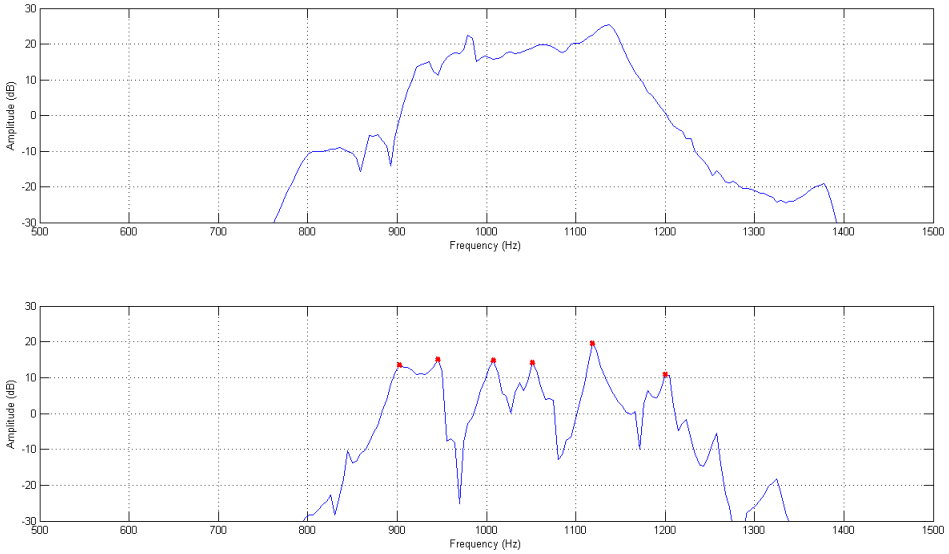

Figure 6.11: Comparison of the passband between the measurements at the 1st (top) and 3rd (bottom) pipe segments

CHAPTER VII

CONCLUSION

1. Summary

This work tried to experimentally study and characterize the propagation of guided acoustic waves in pipe strings interconnected by joints. The ultimate goal of the study was to verify the theoretical results derived by previous works in the scientific literature. In order to achieve this objective, a set of methodical experiments needed to be designed and implemented that can gather robust and reliable data.

First, the existence of the dispersion phenomenon needed to be verified. Second, the instruments used and the experimental setup needed to be checked for consistency of measurements. Once these two tests were successful, the dispersion curves had to be produced and matched with the theoretical curves in order to reinforce the theory, determine the properties of the waveguide, and characterize the dispersion experienced by the acoustic wave. Finally, the response of the pipe strings to different signals and frequencies had to be tested.

2. Main Findings

The first preliminary tests showed that the steel pipe strings can act as a dispersive medium to acoustic waves and that the experimental setup was reliable and produced consistent data. The next round of tests showed that the experimentally produced dispersion curves closely match the theoretical ones. The final tests proved that the pipe strings had several passbands and stopbands in the frequency domain that depend on the number of pipe segments connected. They showed that the reflections and echoes of the acoustic wave arrive at the appropriate times corresponding with the layout of the pipe strings and can add constructively to amplify the signal or destructively to weaken the signal.

REFERENCES

[1] J. L. Rose, "Ultrasonic Waves in Solid Media," Cambridge University Press, Cambridge, UK, 1999.

[2] J. L. Rose, L. Soley, "Ultrasonic guided waves for the detection of anomalies in aircraft components", Materials Evaluation, Vol. 50, No. 9, pg. 1080-1086, 2000.

[3] K. R. Lohr, J. L. Rose, "Ultrasonic Guided Wave and Acoustic Impact Methods for Pipe Fouling Detection", *Journal of Food Engineering*, 56, pp. 315-324, 2002.

[4] J. J. Ditri, J. L. Rose, "Excitation of Guided Elastic Wave Modes in Hollow Cylinders by Applied Surface Tractions," *Journal of Applied Physics*, Vol. 72, No. 7, October 1992.

[5] J. Ma, "On-line measurements of contents inside pipes using guided ultrasonic waves," Ph.D. dissertation, Department of Mechanical Engineering, Imperial College London, London, SW7 2BX, 2007.

[6] D. Alleyne, P. Cawley, "Optimization of Lamb Wave Inspection Techniques", *NDT & E International*, Vol. 25, No. 1, pp. 11–22, 1992.

[7] Y. Gomez-Ullate, F. Espinosa, P. Reynolds, J. Mould, "Selective Excitation of Lamb Wave Modes in Thin Aluminum Plates Using Bonded Piezoceramics: FEM Modeling and Measurement," Poster 205, *European Conference on Non-Destructive Testing – ECNDT*, 2006.

[8] D. S. Drumheller, "An Overview of Acoustic Telemetry," *Proceedings of Geothermal Program Review X – Geothermal Energy and the Utility 120*

Market-The Opportunities and Challenges for Expanding Geothermal Energy in a Competitive Supply Market, San Francisco, CA, USA, pp. 73–79, March 1992.

[9] D. S. Drumheller, "Acoustical Properties of Drill Strings," *The Journal of the Acoustical Society of America*, vol. 85, pp. 1048–1064, March 1989.

[10] D. S. Drumheller, "Wave Impedances of Drill Strings and Other Periodic Media," *The Journal of the Acoustical Society of America*, vol. 112, pp. 2527–2539, December 2002.

[11] D. S. Drumheller and S. D. Knudsen, "The propagation of sound waves in drill strings," *The Journal of the Acoustical Society of America*, 97 (4), pp. 2116-2125, 1995.

[12] D. S. Drumheller, "Attenuation of Sound Waves in Drill Strings," *The Journal of the Acoustical Society of America*, vol. 94, pp. 2387–2396, October 1993.

[13] D. S. Drumheller, "Introduction to Wave Propagation in Nonlinear Fluids and Solids," New York, NY, USA: Cambridge University Press, first ed., 1998.

[14] A. K. Farraj, S. L. Miller, and K. A. Qaraqe, "Propagation Measurements for Acoustic Downhole Telemetry Systems," in *SPE Annual Technical Conference and Exhibition (ATCE)*, New Orleans, LA, USA, pp. 1–24, October 2013.

[15] A. K. Farraj, S. L. Miller, and K. A. Qaraqe, "A Study of Acoustic Wave Propagation inside Cemented Production Tubings," in *International Petroleum Technology Conference*, Doha, Qatar, pp. 1-9, January 2014.

[16] A. K. Farraj, S. L. Miller, and K. A. Qaraqe, "Channel Characterization for Acoustic Downhole Communication Systems," in *SPE Annual Technical*

Conference and Exhibition (ATCE), San Antonio, TX, USA, pp. 1–12, October 2012.

[17] M. S. Kushwaha, "Stop-Bands for Periodic Metallic Rods: Sculptures that can Filter the Noise," Applied Physics Letters, vol. 70, pp. 3218–3220, June 1997.

[18] T. G. Barnes and B. R. Kirkwood, "Passbands for Acoustic Transmission in an Idealized Drill String," *The Journal of the Acoustical Society of America*, vol. 51, pp. 1606–1608, May 1972.

[19] M. P. Horne and R. J. Hansen, "Sound Propagation in a Pipe Containing a Liquid of Comparable Acoustic Impedance," *The Journal of the Acoustical Society of America*, vol. 71, pp. 1400–1405, June 1982.

[20] A. Kondis, "Acoustical Wave Propagation in Buried Water Filled Pipes," Master's thesis, Department of Civil and Environmental Engineering, Massachusetts Institute of Technology, Cambridge, MA, USA, February 2005.

[21] D. E. Weston, "The Theory of the Propagation of Plane Sound Waves in Tube," *Proceedings of the Physical Society*. Section B, vol. 66, pp. 695–709, August 1953.

[22] J. M. Carcione and F. Poletto, "Simulation of Stress Waves in Attenuating Drill Strings, Including Piezoelectric Sources and Sensors," *The Journal of the Acoustical Society of America*, vol. 108, pp. 53–64, July 2000.

[23] S. Sorohan, N. Constantin, M. Gavan, V. Anghel, "Extraction of dispersion curves for waves propagating in free complex waveguides by standard finite element codes", Ultrasonics, 51 503-515, 2011.

[24] T. Pialucha, C.C.H. Guyott, P. Cawley, "Amplitude Spectrum Method for the Measurement of Phase Velocity," Ultrasonics, Vol 27, pp270-279, 1989.

[25] W. Sachse and Y.H. Pao, "On the determination of phase and group velocities of dispersive waves in solids," *Journal of Applied Physics*. 49, 4320-4327, 1978.

[26] J. O. Davies, "Inspection of pipes using low frequency focused guided waves," Ph.D. dissertation, Department of Mechanical Engineering, Imperial College London, London SW7 2AZ, 2008.

[27] A. D. Puckett, "An experimental and theoretical investigation of axially symmetric wave propagation in thick cylindrical waveguides," Ph.D. dissertation, Department of Mechanical Engineering, University of Maine, Orono, ME, May 2004.

[28] D. C. Gazis, "Three-dimensional investigation of the propagation of waves in hollow circular cylinders: I. Analytical foundation," *The Journal of the Acoustical Society of America*, vol.31, pp. 568–573, 1959.

[29] F. Seco and A. Jiménez, "Modelling the generation and propagation of ultrasonic signals in cylindrical waveguides," in Ultrasonic waves, Intech Open Access Publisher, ch. 1, pp. 1-28, 2011.

[30] B. Zaghari, V. Humphrey, M. Moshrefti-Torbati, "Dispersion behavior of torsional guided waves in a small diameter steel gas pipe," *Proceedings of the 19th International Conference on Automation & Computing, Brunel University*, London, UK, 13-14 September 2013.

[31] F. Seco, J. M. Martín, A. R. Jiménez, J. L. Pons, L. Calderón, R. Ceres, "PCDISP: a tool for the simulation of wave propagation in cylindrical waveguides", *Ninth International Congress on Sound and Vibration*, Orlando, Florida, 2002.

[32] S. M. Ziola and M. R. Gorman, "Experimental Plate Wave Dispersion Analysis," *Review of Progress in Quantitative Nondestructive Evaluation*, 10B, 1991.

[33] P. Horaa and O. Cervena, "Determination of Lamb wave dispersion curves by means of Fourier transform", Applied and Computational Mechanics 6, pp. 5-16, 2012.

[34] D. Alleyne and P. Cawley, "A 2-dimensional Fourier transform method for the quantitative measurement of Lamb modes, " in: D.O. Thompson, D.E. Chimenti (Eds.), *Review of Progress in Quantitative Nondestructive Evaluation*, Vol. 10A, pp. 201–208, 1991.

APPENDIX A

The entries of the displacement and stress matrices derived in [29, 30] are found to be:

$$D_u(1,1) = nW_n(\alpha r) - \alpha W_{n+1}(\alpha r) \tag{A.1}$$

$$D_u(1,2) = nZ_n(\alpha r) - \lambda_1 \alpha Z_{n+1}(\alpha r) \tag{A.2}$$

$$D_u(1,3) = krW_{n+1}(\beta r) \tag{A.3}$$

$$D_u(1,4) = krZ_{n+1}(\beta r) \tag{A.4}$$

$$D_u(1,5) = nW_n(\beta r) \tag{A.5}$$

$$D_u(1,6) = nZ_n(\beta r) \tag{A.6}$$

$$D_u(2,1) = jnW_n(\alpha r) \tag{A.7}$$

$$D_u(2,2) = jnZ_n(\alpha r) \tag{A.8}$$

$$D_u(2,3) = -jkrW_{n+1}(\beta r) \tag{A.9}$$

$$D_u(2,4) = -jkrZ_{n+1}(\beta r) \tag{A.10}$$

$$D_u(2,5) = jnW_n(\beta r) - j\beta rW_{n+1}(\beta r) \tag{A.11}$$

$$D_u(2,6) = jnZ_n(\beta r) - j\lambda_2 \beta rZ_{n+1}(\beta r) \tag{A.12}$$

$$D_u(3,1) = jkrW_n(\alpha r) \tag{A.13}$$

$$D_u(3,2) = jkrZ_n(\alpha r) \tag{A.14}$$

$$D_u(3,3) = j\lambda_2 \beta rW_n(\beta r) \tag{A.15}$$

$$D_u(3,4) = j\beta Z_n(\beta r) \tag{A.16}$$

$$D_u(3,5) = 0 \tag{A.17}$$

$$D_u(3,6) = 0 \tag{A.18}$$

$$D_\sigma(1,1) = \big((k^2-\beta^2)r^2 + 2(n-1)\big)W_n(\alpha r) + 2\alpha r W_{n+1}(\alpha r) \quad \text{(A.19)}$$

$$D_\sigma(1,2) = \big((k^2-\beta^2)r^2 + 2(n-1)\big)Z_n(\alpha r) + 2\lambda_1 \alpha r Z_{n+1}(\alpha r) \quad \text{(A.20)}$$

$$D_\sigma(1,3) = 2\lambda_2 \beta k r^2 W_n(\beta r) - 2(n+1)krW_{n+1}(\beta r) \quad \text{(A.21)}$$

$$D_\sigma(1,4) = 2\beta k r^2 Z_n(\beta r) - 2(n+1)krZ_{n+1}(\beta r) \quad \text{(A.22)}$$

$$D_\sigma(1,5) = 2n(n-1)W_n(\beta r) - 2n\beta r W_{n+1}(\beta r) \quad \text{(A.23)}$$

$$D_\sigma(1,6) = 2n(n-1)Z_n(\beta r) - 2n\lambda_2 \beta r Z_{n+1}(\beta r) \quad \text{(A.24)}$$

$$D_\sigma(2,1) = ((2\alpha^2-\beta^2+k^2)r^2 - 2n(n-1))W_n(\alpha r) - 2\alpha r W_{n+1}(\alpha r) \quad \text{(A.25)}$$

$$D_\sigma(2,2) = ((2\alpha^2-\beta^2+k^2)r^2 - 2n(n-1))Z_n(\alpha r) - 2\lambda_1 \alpha r Z_{n+1}(\alpha r) \quad \text{(A.26)}$$

$$D_\sigma(2,3) = 2(n+1)krW_{n+1}(\beta r) \quad \text{(A.27)}$$

$$D_\sigma(2,4) = 2(n+1)krZ_{n+1}(\beta r) \quad \text{(A.28)}$$

$$D_\sigma(2,5) = -2n(n-1)W_n(\beta r) - 2n\beta r W_{n+1}(\beta r) \quad \text{(A.29)}$$

$$D_\sigma(2,6) = -2n(n-1)Z_n(\beta r) - 2n\lambda_2 \beta r Z_{n+1}(\beta r) \quad \text{(A.30)}$$

$$D_\sigma(3,1) = (2\alpha^2-\beta^2-k^2)r^2 W_n(\alpha r) \quad \text{(A.31)}$$

$$D_\sigma(3,2) = (2\alpha^2-\beta^2-k^2)r^2 Z_n(\alpha r) \quad \text{(A.32)}$$

$$D_\sigma(3,3) = -2\lambda_2 \beta k r^2 W_n(\alpha r) \quad \text{(A.33)}$$

$$D_\sigma(3,4) = -2\beta k r^2 Z_n(\alpha r) \quad \text{(A.34)}$$

$$D_\sigma(3,5) = 0 \quad \text{(A.35)}$$

$$D_\sigma(3,6) = 0 \quad \text{(A.36)}$$

$$D_\sigma(4,1) = -2nkrW_n(\alpha r) \quad \text{(A.37)}$$

$$D_\sigma(4,2) = -2nkrZ_n(\alpha r) \tag{A.38}$$

$$D_\sigma(4,3) = kr^2W_{n+1}(\beta r) - \lambda_2 n\beta r W_n(\beta r) \tag{A.39}$$

$$D_\sigma(4,4) = kr^2Z_{n+1}(\beta r) - n\beta r Z_n(\beta r) \tag{A.40}$$

$$D_\sigma(4,5) = -nkrW_n(\beta r) + \beta kr^2W_{n+1}(\beta r) \tag{A.41}$$

$$D_\sigma(4,6) = -nkrZ_n(\beta r) + \lambda_2\beta kr^2Z_{n+1}(\beta r) \tag{A.42}$$

$$D_\sigma(5,1) = 2jnkrW_n(\alpha r) - 2jk\alpha r^2W_{n+1}(\alpha r) \tag{A.43}$$

$$D_\sigma(5,2) = 2jnkrZ_n(\alpha r) - 2j\lambda_1 k\alpha r^2Z_{n+1}(\alpha r) \tag{A.44}$$

$$D_\sigma(5,3) = j\lambda_2 n\beta r W_n(\beta r) - j(\beta^2 - k^2)r^2W_{n+1}(\beta r) \tag{A.45}$$

$$D_\sigma(5,4) = jn\beta r Z_n(\beta r) - j(\beta^2 - k^2)r^2Z_{n+1}(\beta r) \tag{A.46}$$

$$D_\sigma(5,5) = jnkrW_n(\beta r) \tag{A.47}$$

$$D_\sigma(5,6) = jnkrZ_n(\beta r) \tag{A.48}$$

$$D_\sigma(6,1) = 2jn(n-1)W_n(\alpha r) - 2jn\alpha r W_{n+1}(\alpha r) \tag{A.49}$$

$$D_\sigma(6,2) = 2jn(n-1)Z_n(\alpha r) - 2jn\lambda_1\alpha r Z_{n+1}(\alpha r) \tag{A.50}$$

$$D_\sigma(6,3) = -j\lambda_2\beta kr^2W_n(\beta r) + 2jkr(n+1)W_{n+1}(\beta r) \tag{A.51}$$

$$D_\sigma(6,4) = -j\beta kr^2Z_n(\beta r) + 2jkr(n+1)Z_{n+1}(\beta r) \tag{A.52}$$

$$D_\sigma(6,5) = j(2n(n-1) - \beta^2r^2)W_n(\beta r) + 2j\beta r W_{n+1}(\beta r) \tag{A.53}$$

$$D_\sigma(6,6) = j(2n(n-1) - \beta^2r^2)Z_n(\beta r) + 2j\lambda_2\beta r Z_{n+1}(\beta r) \tag{A.54}$$

All the entries of the displacement matrix are scaled by $\frac{1}{r}$ while all the entries of the stress matrix are scaled by $\frac{G}{r^2}$ with G being the shear modulus of the material. The parameters α and β are defined as:

$$\alpha = \frac{\omega^2}{c_l^2} - k^2 \tag{A.55}$$

$$\beta = \frac{\omega^2}{c_s^2} - k^2 \tag{A.56}$$

c_l and c_s are the respective longitudinal and shear velocities of the waveguide, and $\omega = 2\pi f$ being the angular frequency. The rest of the parameters are defined by Table A.1 [29, 30]:

Table A.1: Choice of parameters for the determinant equation solution

Frequency Range	Coefficients	Bessel Functions	Wavenumber
$\frac{\omega}{k} < c_r$	$\alpha^2, \beta^2 < 0$ $\lambda_1 = \lambda_2 = -1$	$Z_n(\alpha r) = I_n(\alpha r)$ $W_n(\alpha r) = K_n(\alpha r)$ $Z_n(\beta r) = I_n(\beta r)$ $W_n(\beta r) = K_n(\beta r)$	Real
$c_r < \frac{\omega}{k} < c_l$	$\alpha^2 < 0, \beta^2 > 0$ $\lambda_1 = -1, \lambda_2 = 1$	$Z_n(\alpha r) = I_n(\alpha r)$ $W_n(\alpha r) = K_n(\alpha r)$ $Z_n(\beta r) = J_n(\beta r)$ $W_n(\beta r) = Y_n(\beta r)$	Real
$\frac{\omega}{k} > c_l$	$\alpha^2, \beta^2 > 0$ $\lambda_1 = \lambda_2 = 1$	$Z_n(\alpha r) = J_n(\alpha r)$ $W_n(\alpha r) = Y_n(\alpha r)$ $Z_n(\beta r) = J_n(\beta r)$ $W_n(\beta r) = Y_n(\beta r)$	Real
Any	$\alpha^2, \beta^2 > 0$ $\lambda_1 = \lambda_2 = 1$	$Z_n(\alpha r) = J_n(\alpha r)$ $W_n(\alpha r) = Y_n(\alpha r)$ $Z_n(\beta r) = J_n(\beta r)$ $W_n(\beta r) = Y_n(\beta r)$	Imaginary